2017

A Thermally Stabilized Fluorescent Organic Chromophore

Brendan P. Hughes
Binghamton University--SUNY, bhughe10@binghamton.edu

A THERMALLY STABILIZED FLUORESCENT ORGANIC CHROMOPHORE

BY

BRENDAN PATRICK HUGHES

BS, University at Buffalo, 2014

THESIS

Submitted in partial fulfillment of the requirements for
the degree of Master of Science in Chemistry
in the Graduate School of
Binghamton University
State University of New York
2017

Accepted in partial fulfillment of the requirements for
the degree of Master of Science in Chemistry
in the Graduate School of
Binghamton University
State University of New York
2017

December 4, 2017

Prof. Nikolay Dimitrov, Chair and Faculty Advisor
Department of Chemistry, Binghamton University

Prof. M. Stanley Whittingham, Examiner
Department of Chemistry, Binghamton University

Prof. Chuan-Jian Zhong, Examiner
Department of Chemistry, Binghamton University

ABSTRACT

A fluorescent chromophore, hereby designated as cyanine dye, has been bound to generated zinc oxide nanoparticles. It has been shown that the material not only retains the characteristic absorption peak of the native chromophore, but it also continues to fluoresce with comparable intensity. The binding occurs through a Zn – O_2C bridge, which allows for vibrational relaxation as the dye heats up, yet also preserves the optical properties of the dye. This bond linkage can be observed from the comparison of FT-IR spectra of the nanoparticles and the native dye, designated by a shift in one of the peaks at 1730 cm^{-1}. The nanoparticle-dye material has been characterized through a variety of techniques, including differential scanning calorimetry, thermal gravimetric analysis, scanning electron microscopy, and energy-dispersive X-ray spectroscopy. The thermal stability of the dye was improved from a significant level of decomposition by 200 ºC to nearly no loss of mass at 350 ºC. It proved impossible to record a Raman spectrum of the dye itself, as the laser degraded the dye before measurements could be taken, but the thermal stabilization of the nanomaterial also allowed the dye to be examined by Raman spectroscopy without decomposition. Both the dye and the nanomaterial exhibit the same Stokes shift, from the 819 nm absorbance peak to an 850-nm emission peak.

ACKNOWLEDGEMENTS

I want to thank Dr. Wayne E. Jones Jr. for standing up on my behalf to continue research with Binghamton University. If not for his intervention, I would not have made the same progress I have today. He is constantly attending meetings and fielding questions and requests from people on and off campus. However, he still found the time to check in on my progress and make sure I was on the right track, and he always responded to my questions and concerns. I owe him a debt of gratitude for this opportunity to continue my studies at Binghamton.

Credit for the synthetic processes employed goes to Dr. Kenneth Skorenko, for initially developing the methods listed in this thesis. Without his guidance and support of my lab work, I would have struggled much harder and achieved much less.

It would be remiss if I did not properly thank Wei Wu, Dr. Linyue Tong, and Dr. Steve Boyer for their contributions to my project. Wei was generous enough to synthesize ZnO nanoparticles, and both Dr. Tong and Dr. Boyer performed characterizations on my samples while working on their own projects.

Finally, I would like to thank both Binghamton University and Crysta-Lyn Chemical Company for providing me the resources to conduct the research described in this thesis. Binghamton's new Center of Excellence and Crysta-Lyn's dyes and characterizations were critical to the success of this work.

TABLE OF CONTENTS

LIST OF FIGURES

INCREASED THERMAL STABILITY OF ORGANIC FLUORESCENT CHROMOPHORE WITH NANOPARTICLE ZNO

1. Introduction

Organic dyes, synthesized or refined from natural sources, have always been a feature of human society. Since it was discovered that berries could be squeezed for their colored juices, people have stained clothing, leather, and other fabrics with these dyes.[24] For best effect, they were worked with at high temperatures, but if too much heat was applied, the dye would decompose and simply wash out. For this reason, ZnO nanoparticles have been synthesized in situ and dye molecules bound to them to enhance thermal stability.

Dyes have a wide variety of applications. From sensors to colorants to fluorophores, they have been applied to many fields of research in different roles. For instance, they have been used to create thermally sensitive coating for printing-press technology. As many printers now operate in the CTP format (computer to plate); i.e. the design is created digitally and then transferred to the plate via an infrared laser.

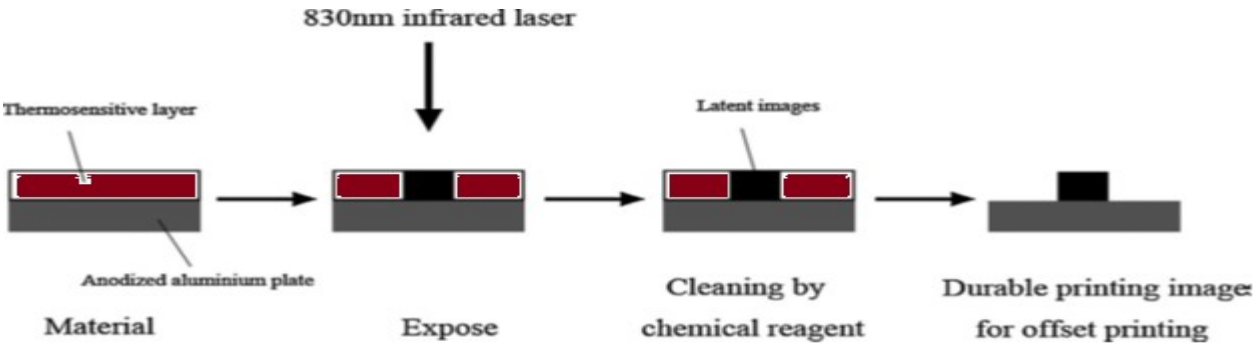

Figure 1. CTP imaging process, with dye indicated in red.[1]

The problem with this process is that the images generated by the laser are not ready for printing, and traditional development processes generate a large amount of pollution by using chemical reagents.[1] Essentially, there is a strong environmental need for a dye that will properly respond to the infrared laser to create latent images without chemical development. Simple infrared-absorbing dyes are perfectly capable of absorbing 830 nm light, but the energies they are exposed to require thermal release after absorption. In this particular case, thermal activation causes polymerization of monomer nanoparticles mixed with the dye, generating a clean latent image in the plate. This represents another example of the use of nanoparticles to manage thermal buildup in dye molecules. Additionally, work has been conducted to improve the thermal stability of a dye by simply exchanging the counter-anion from iodide to multi-fluoride anions, such as PF_6^-.

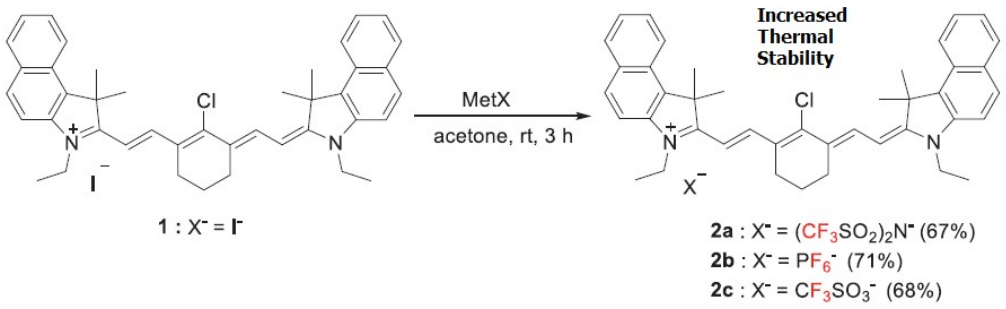

Figure 2. Counter-anion substitution of heptamethine cyanine dyes 2a-c.[2]

As they are counter-ions, they play no part in the covalent bonding, which gives the dye its character. This approach involves replacing iodide with a molecular anion with a high fluorine content, and a significantly lower oxidation potential, decreasing the chances of oxidizing the dye. Accordingly, there is a small loss in the fluorescent quantum yield, however, this is minimal compared to the increased thermal stability, which is typically an additional 20-50 ºC above the original decomposition temperature.[2]

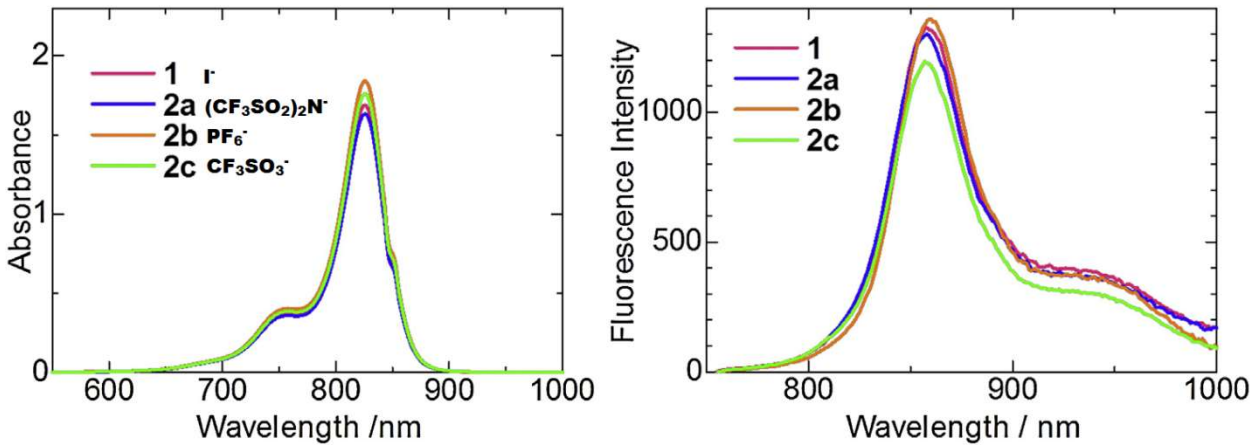

Figure 3. UV-Vis absorption and fluorescence spectra of cyanine dyes with indicated counter-ions.[2]

Fluorescence can be analyzed using a variety of parameters in order to image dynamically a particular mechanism. Two methods available are photoinduced electron transfer (PET), and fluorescence resonance energy transfer (FRET). PET is capable of measuring van der Waals contact formation rates of a fluorescent dye with a fluorescence quencher,[7] allowing the dynamics of fluorescence quenching to be analyzed. FRET, on the other hand, can examine the non-radiative transfer of excited electrons from donor to acceptor between 2 and 10 nm. The results it yields can reveal the relative orientation factor of the two electronic transition dipole vectors in question. Combining these two imaging techniques can reveal the dynamics of fluorophore function on a molecular level, giving greater insight into the means by which excited electrons are permitted to emit photons.

Fluorophores have also been applied as bio-imaging contrast agents; specifically fluorescent dyes have been doped into nanoparticles for the purposes of imaging *in vivo*. If a nanoparticle is non-toxic, like ZnO, then it can be paired with a fluorophore and

injected into living tissue. Depending on the absorption/emission characteristics of the dye, various depths of penetration into living tissue can be attained, and fluorescence can be observed from internal organs. This allows for some tantalizing opportunities in medicine, as there are few other methods for imaging the internal ecosystem of an organism without disturbing it or potentially harming the organism, as with X-rays. MRI and ultrasound are capable of imaging internal mechanisms without the risk of damage, but their efficiency is limited by the need for contrast agents. A fluorophore which can bind selectively to tumors, for instance, could be used to locate them without invasive techniques. Generally speaking, green fluorescent protein (GFP) is one of the most common fluorophores, on account of its visible excitation wavelength and minimal degree of photobleaching.[6] If GFP is attached to a selectively-binding carrier group which readily cleaves once inside the cell membrane (such as a pH-low insertion peptide (pHLIP)), fluorescent imaging of tumors becomes inexpensive and highly specific.[17] Moreover, this technique is not limited to non-invasive bio-imaging. Especially if the fluorescent characteristic peak is outside the visible spectrum, fluorescence can be used to label anything compatible with dyes in a way which can be easily measured, yet not easily discovered by accident. The ability to label something with a fluorophore that is only visible using special optics, such as infrared imaging, is potentially useful on today's battlefields to identify friend or foe. If the quantum yield of the fluorophore is sufficient, it will effectively allow the label to be visible over 360º, which is significantly better than other labelling methods which utilize scattering. While scattering has a high quantum yield (almost 1), it is only visible at a very narrow angle, requiring the optics to be aligned precisely.

In particular, organic cyanine chromophores have been used in a variety of applications. However, they are limited by thermal and photo stability, both of which are poor. Therefore, while they are useful for light filtration, bio-imaging, photovoltaics, and clothing color control, they cannot be used in more intensive applications such as laser filtration, electronic displays, or solar devices. The advantage of cyanine dyes for such applications is the high degree of customization that can be exploited to tailor the absorbing wavelength. Modification of the two end groups and the conjugated bridge can tune the potential electron transitions to either more confined (blue shift) or expanded (red shift) quantum domains.[3,8,10]

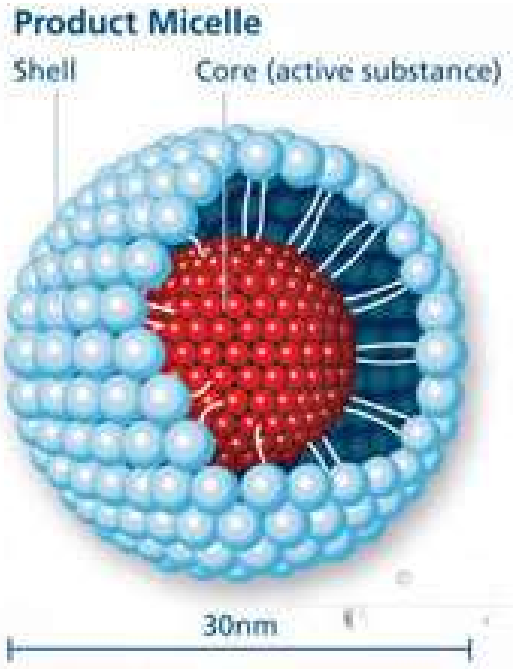

Figure 4. Structure of a micelle-dye core-shell macromolecule.

There are many existing methods for stabilization of dyes, all with their own benefits and drawbacks. One of the most common methods used in the past is to synthesize micelles in an aqueous solution, which are essentially spheres of emulsifier

molecules, made spherical by the amphiphilic nature of the emulsifier (Figure 4). The water-soluble portions of the molecules naturally gravitate towards the outside of the micelles, while the hydrophobic parts tend to withdraw into themselves, naturally creating water-soluble spheres. This method not only improves thermal stability, but also prevents aggregation by confining the dye molecules to the inside of the micelles. However, the major drawback of this process is the large amount of detergent required in the process, generally requiring a 1:10 molar ratio between dye and detergent.[25]

Another method being developed is the replacement of counter-anions with colorless naphthalenedisulfonate anions bound to functional groups capable of hydrogen bonding, such as –OH groups. This method, so far, is specific to optical discs like CDs, requiring that the dye react to heat supplied by an intensity-modulated laser in order to record a signal, yet remain unchanged by the environment after recording. After exposure to the laser, the dye is thermally deformed, causing it to complex into a network of hydrogen bonds with its colorless counter-anion. This not only prevents thermal breakdown from occurring, but stabilizes the molecules to the point where they won't crystallize over time: another degradation pathway for optical discs.[27] While this is a viable process, it has a chance to discolor the dye as well as introducing more toxic chemicals to the product, and eventually, the environment.

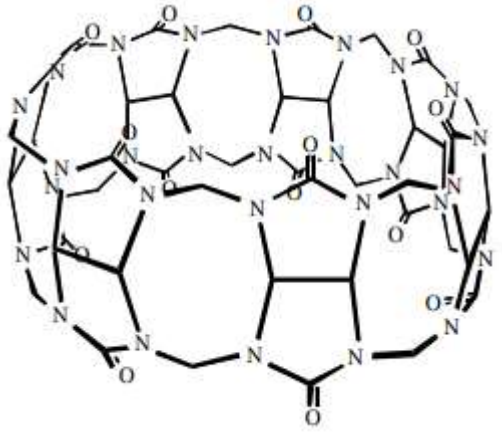

Figure 5. Cucurbit[7]uril (CB7) molecular structure.[28]

One method of thermal stabilization which not only produces results, but also has a chance to enhance the photophysical properties of the dye being examined, is use of a molecule known as cucurbit[7]uril, or CB7, pictured in Figure 5. This large molecule encapsulates the dye inside its structure in a 1:1 or 2:1 molar ratio of CB7 to dye, binding with most dyes except ones containing sulfonate groups. Many the dyes tested with this molecule have been fluorescent. In most cases, the quantum yield of the fluorescent dyes were either preserved or improved, with similar increases being witnessed with respect to the dye's extinction coefficient and brightness. One of the major weaknesses of this method, however, is that the dye must be water soluble for this process to work efficiently. Most IR absorbing dyes are sparingly soluble in water, if at all.[28] As this project pertains to an IR absorbing dye, this method cannot be employed.

Currently, thermally stabilized cyanine dyes have been designated for developments to protect the safety of pilots. Dazzling pilots using laser pointers is increasingly becoming a safety concern. This can result in a large distance being flown completely blind. This may be mitigated using visors containing a laminated dye

nanomaterial, made with a designer cyanine dye coupled with ZnO nanoparticles to withstand the melting process necessary to make it into a glass. The binding of dye to nanoparticle occurs through a carboxyl-zinc bond, pictured in Figure 6.

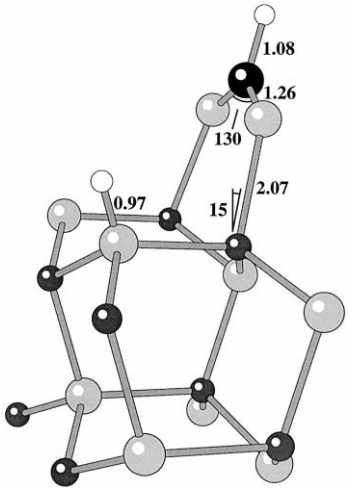

Figure 6. Binding of carbonyl COO^- to Zn atoms in ZnO.[29]

Through a facile electrochemical synthetic process, the dye may be affixed to ZnO nanoparticles, stabilizing the dyes to temperatures of about 300 ºC, some 150 ºC higher than for the naked dye. This process affects the chemistry of the dye itself, in particular the way it interacts with light. The question is: to what extent are the original dye properties preserved? Applications of an infrared-fluorescent dye, such as cyanine dye, include many military uses, such as identifying friend-or-foe. Due to the nature of cyanine dyes, this process does not affect the chemistry significantly and may be directed to any wavelength desired using a variety of dyes bound to ZnO nanoparticles, allowing for the whole infrared spectrum to be accessed. This process requires melt-extrusion of polymer fibers incorporating laminated dye nanomaterial into the special woven patches

on the soldiers' clothing, so heat stability is essential to withstand the elevated temperatures of extrusion.

As a semiconductor, ZnO will not interfere with conductivity as much as an insulator, yet will still not act as a fully conductive metal. In the applications of thermally stabilizing a cyanine dye it is ideal, as it has a bandgap suitable to absorb the vibrational energies of heating. The 3.37 eV bandgap ensures that electronic transitions are thermally inaccessible, in contrast to pure metals, which fluoresce when heated. This is, however, a trait of most semiconductors, so why zinc oxide? When speaking of chromophores, any absorbance peaks in the spectrum aside from the characteristic one will introduce unwanted absorption of light, which is exactly what we wish to avoid. ZnO is transparent to visible light and can be made highly conductive by doping.[19] The white color of ZnO is fully compatible with dyes, as it does not interfere with the absorption spectrum so long as particles do not approach a size to physically scatter visible light. The fact that ZnO is already conductive, which can be improved with simple modifications, means that the electronic structure of the dye is likely to remain unchanged, as shown by the UV-Vis spectra in Figure 7.

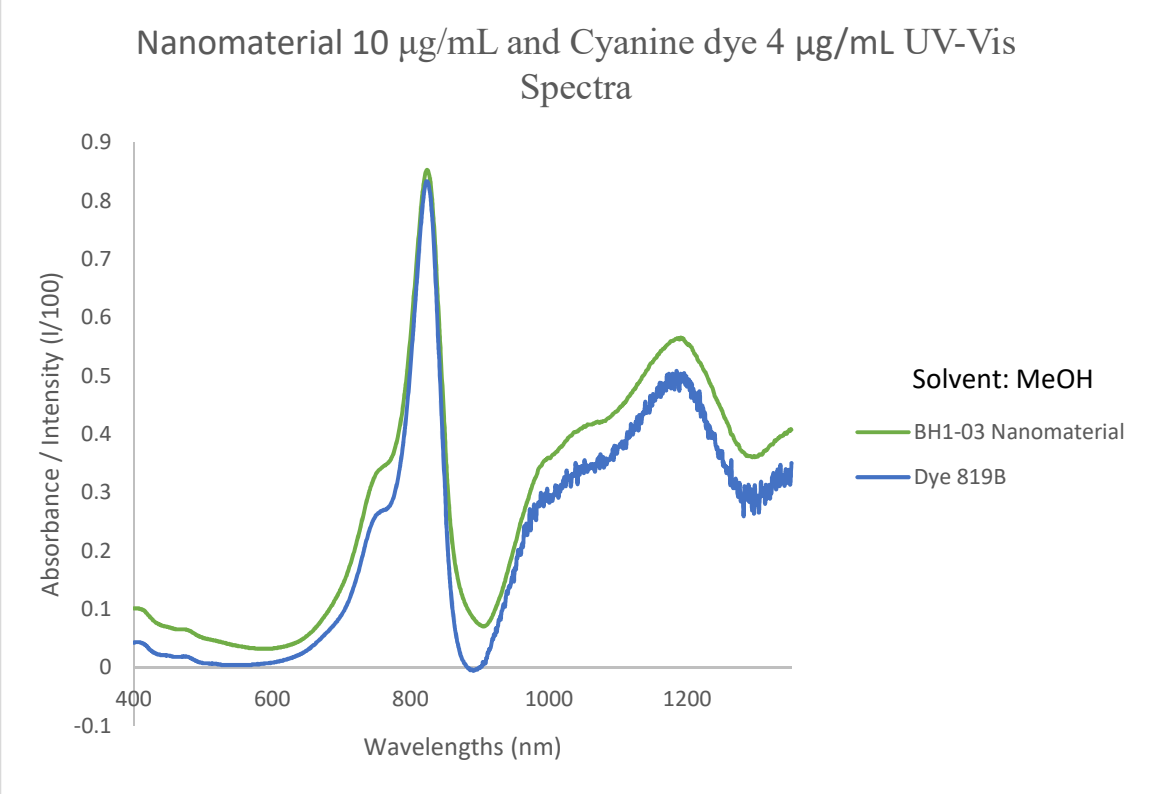

Figure 7. Comparative UV-Vis spectra of cyanine dye and 1.0 mM dye nanomaterial.

Finally, ZnO can bind to the dye without altering the dye molecule structure significantly as it does not perturb any sites associated with the chromophore. Instead, the oxophilicity of zinc causes it to bind to the carboxylate functionality of the dyes. This lies outside the chromophore (Figure 8). Most cyanine dye with similar COO^{-} groups can be stabilized using this approach, opening up a wide range of designer dyes which may be inexpensively stabilized. In this thesis, only one cyanine dye will be discussed.

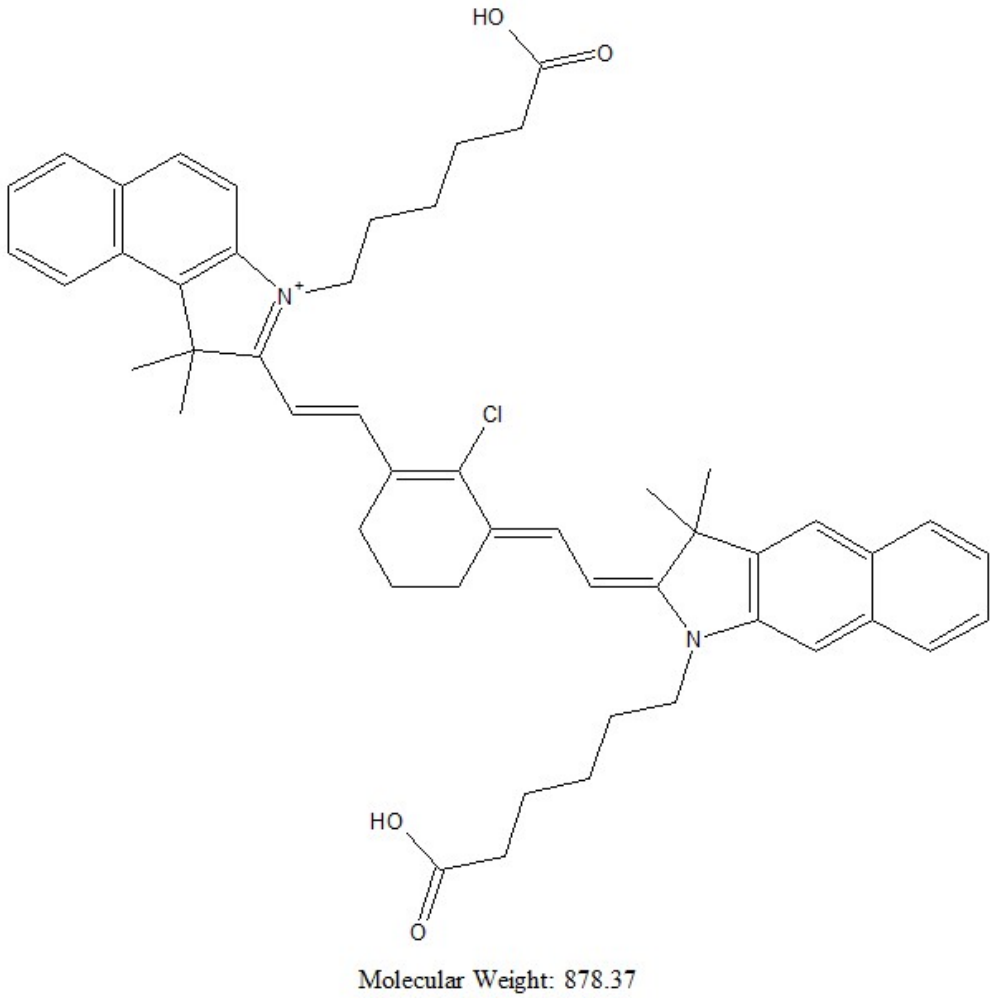

Figure 8. Molecular structure of cyanine dye.

2. Experimental

2.1. **Materials**

Zinc metal and stainless steel foil (Type 304) were purchased from Alpha Aesar and cut into electrodes of various sizes, suitable for the reaction vessels used in electrochemical decomposition. Dyes were donated by Crysta-Lyn Chemical Company,

Inc. and used as received. All other solvents and chemicals were reagent grade, purchased from Sigma Aldrich and used as received.

2.2. **Generation of Nanomaterial**

The ZnO nanoparticles were generated via electrochemical decomposition carried out under oxidizing conditions. Zn metal (99.999%) was used as a sacrificial anode and porous stainless steel (Type 304) as a cathode. Both electrodes were immersed in a solution of 0.1 M tetrabutylammonium bromide (TBAB) in isopropanol, with chromophore (cyanine dye) dissolved in solution to 1.0 mM. For the batch designated 0.1 mM dye, only 0.1 mM of cyanine dye was utilized. 1.0 mM dye used a full concentration of 1.0 mM cyanine dye. Using a Keithley SourceMeter 2400, current was applied between the electrodes at a fixed potential of 30 V. Oxygen was supplied to the system at a steady rate of 1.2 mL/min by bubbling it into the bottom of the reaction vessel. The process was continued for 4 h, producing a dark green nanomaterial. In the absence of dye, the ZnO nanoparticles deposit as pure white powder. Three batches of the nanoparticles were prepared with varying concentrations of surfactant (0.05 M TBAB, 0.1 M TBAB, and 0.5 M TBAB).

Once synthesis was completed, the solution was repeatedly filtered through a fritted Buchner funnel with pores < 200 nm, washed with methanol and sonicated, then re-filtered until the filtrate attained the consistency of a fine powder, with minimal trace amounts of TBAB and dye remaining. Residual TBAB, as well as the drying process itself, caused aggregation of the nanomaterial, which required a mortar and pestle to grind back to fine powder.

2.3 **Instrumentation**

Thermal Gravimetric Analysis (TGA) coupled with Differential Scanning Calorimetry (DSC) was used to analyze the thermal stability of the ZnO nanoparticles, dye, and dye-coupled nanomaterial. A Thermal Instruments TGA Series Q50 was utilized in isothermal mode, which was set to activate with sample mass changes greater than 1% and deactivate when mass change fell below 0.05%.

Scanning Electron Microscopy (SEM) images were taken on a Zeiss Supra 55VP with attached EDAX facility, using an in-lens microscope. Samples were coated in 7-11 nm of conductive carbon. The EDAX was also used to provide an elemental analysis for the samples prepared.

Fourier Transform Infrared (FT-IR) spectra were previously recorded of 0.1 mM dye nanomaterial, as well as cyanine dye and ZnO nanoparticles. Additionally, TEM images were measured for 0.1 mM dye and 1.0 mM dye nanomaterial.

A Shimadzu FT-IR spectrophotometer was utilized, as well as a UV-Vis spectrophotometer and Fluorimeter (also Shimadzu). For FT-IR analysis, 1.0 mM dye nanomaterial sample was ground into a KBr pellet and examined; in the UV-Vis and Fluorimeter, 0.1 mg/mL stock solutions of ZnO, cyanine dye, and nanomaterial were prepared. ZnO and nanomaterial suspensions were then diluted by 10x for a final concentration of 10 μg/mL, while the dye required further dilution down to 4 μg/mL in order to register an absorbance maximum less than 1. All solutions used in the spectrophotometers were prepared with methanol solvent. UV-Vis spectra spanned the range 400-1350 nm, while fluorimetry was performed with an excitation wavelength of

820 nm and covered the range of 820-900 nm, as the emission maximum was expected to occur less than 100 nm from the absorbance peak at 819 nm. The 900 nm upper range represented the limit of the capability of the instrument.

3. Results and Discussion

3.1. **Thermal Gravimetric Analysis (TGA)/Differential Scanning Calorimetry (DSC)**

As this project is focused on thermally stabilizing dyes with nanoparticles, TGA is one of the most important analytical methods, as it determines the threshold(s) of thermal breakdown. Samples of cyanine dye, ZnO nanoparticles, and the combined nanomaterial were all tested using TGA. Additionally, DSC scans of the dye and the nanomaterial were performed and analyzed.

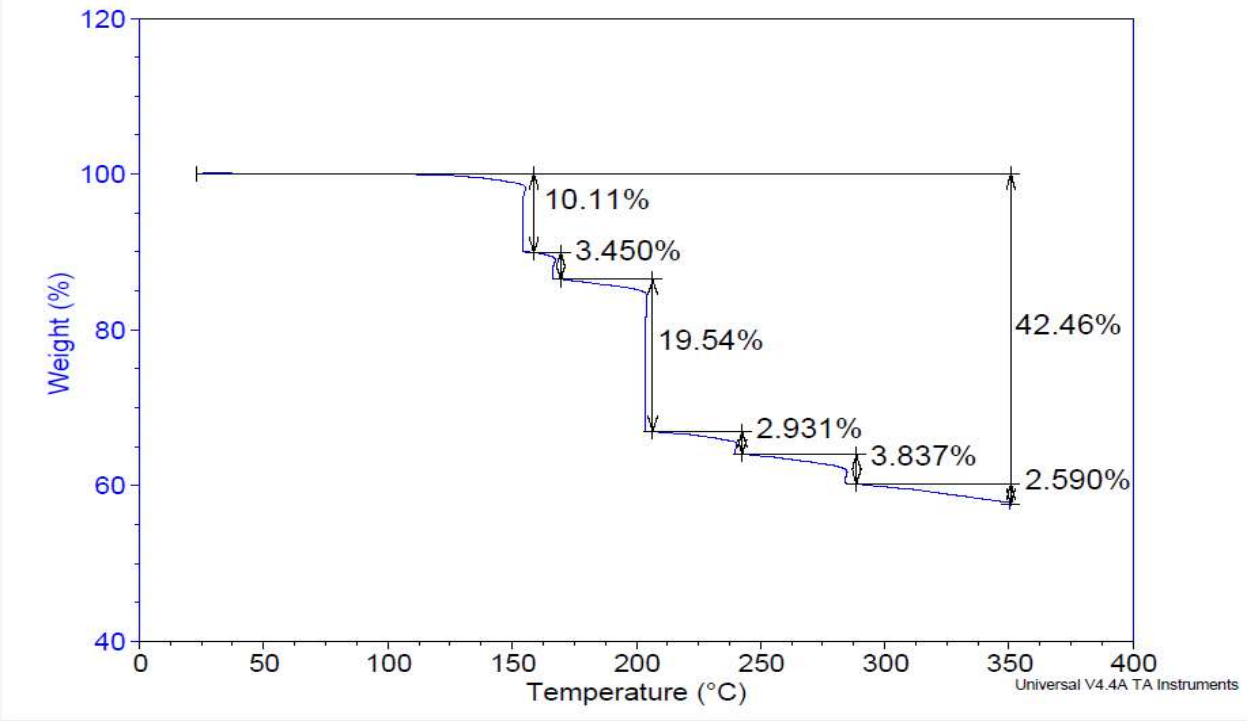

Figure 1.1 TGA plot of cyanine dye, scanned at 7 ºC/min.

As seen in Figure 1.1, a pure sample of cyanine dye lost 42.46% of its total mass by 350 ºC, with the largest individual losses occurring at about 150 ºC and 200 ºC, losing 10% and 20%, respectively. This indicates the dye loses the vast majority of its mass between 150 ºC and 200 ºC, which is fairly normal for a cyanine dye of this grade. The dye likely loses its tertiary methyl groups first, as they are small enough to correspond to the initial mass loss, followed by the long carboxylic acid chains around 200 ºC on account of their relative lack of stability and large contribution to the molecular weight.

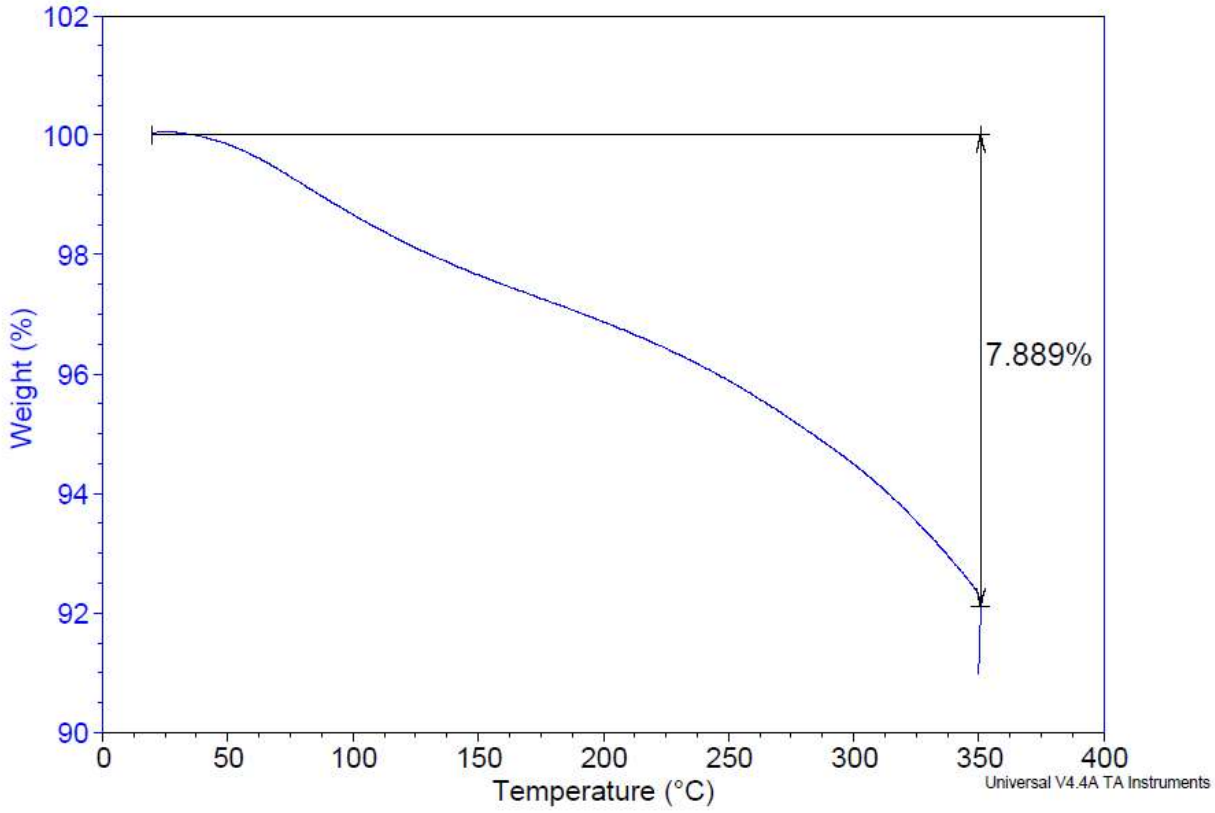

Figure 1.2 TGA plot of cyanine dye Nanomaterial (0.1 mM dye).

In contrast, the dye nanomaterial never showed a mass loss greater than 1%, and exhibited no isotherms. By the end of the analysis at 350 ºC, it had lost only 8% of its total mass; a vast improvement over the naked dye. There does not appear to be any

particular temperature where major losses occur; rather, the loss of mass seems to be gradual and nearly linear from 50 ºC to 350 ºC. Since the carboxylic acid chains are protected by the ZnO binding, it is most likely this mass loss stems from the tertiary methyl groups.

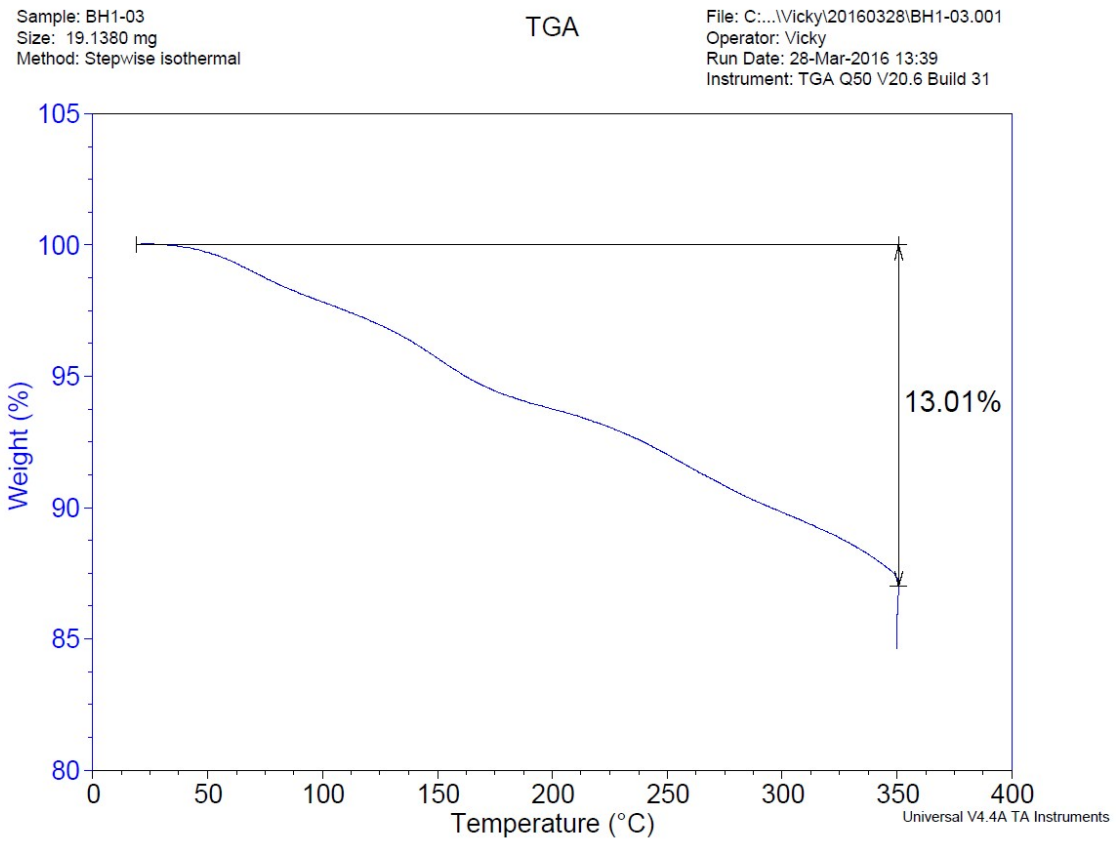

Figure 1.3 TGA plot of 1.0 mM dye nanomaterial.

The nanomaterial with a full concentration of dye used in its preparation predictably loses more of its mass between 0 and 350 ºC. The organic dye is the thermally sensitive component, so the higher the dye concentration, the more mass should be lost with heating. However, there are plateaus midway through the TGA that were absent in 0.1

mM dye, most likely because the sample of 1.0 mM dye which was analyzed has a higher concentration of dye.

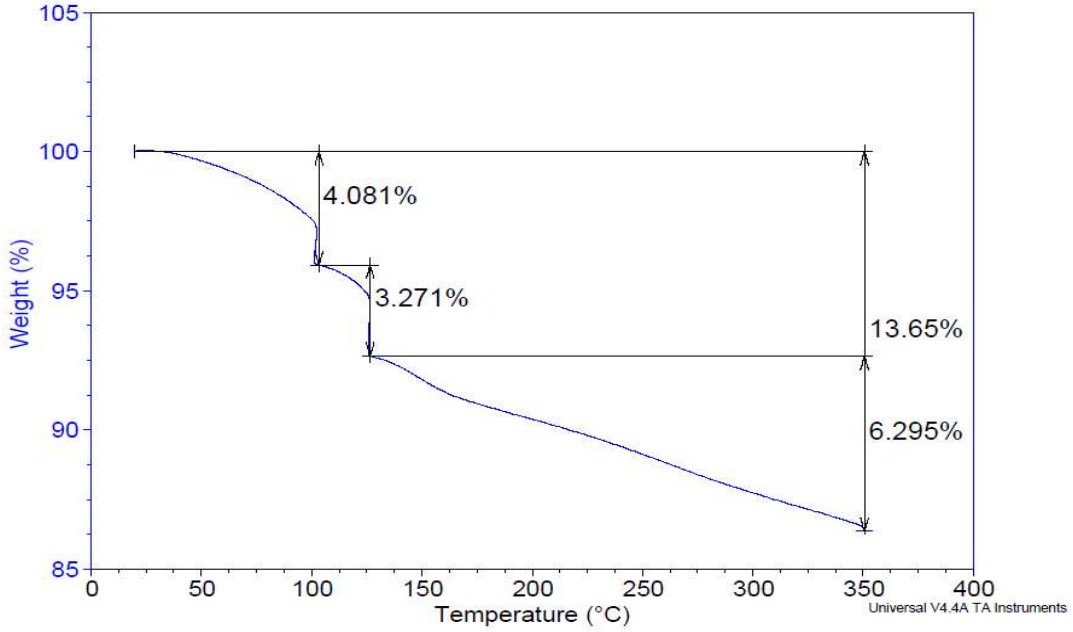

Figure 1.4 TGA plot of ZnO (0.1 M TBAB).

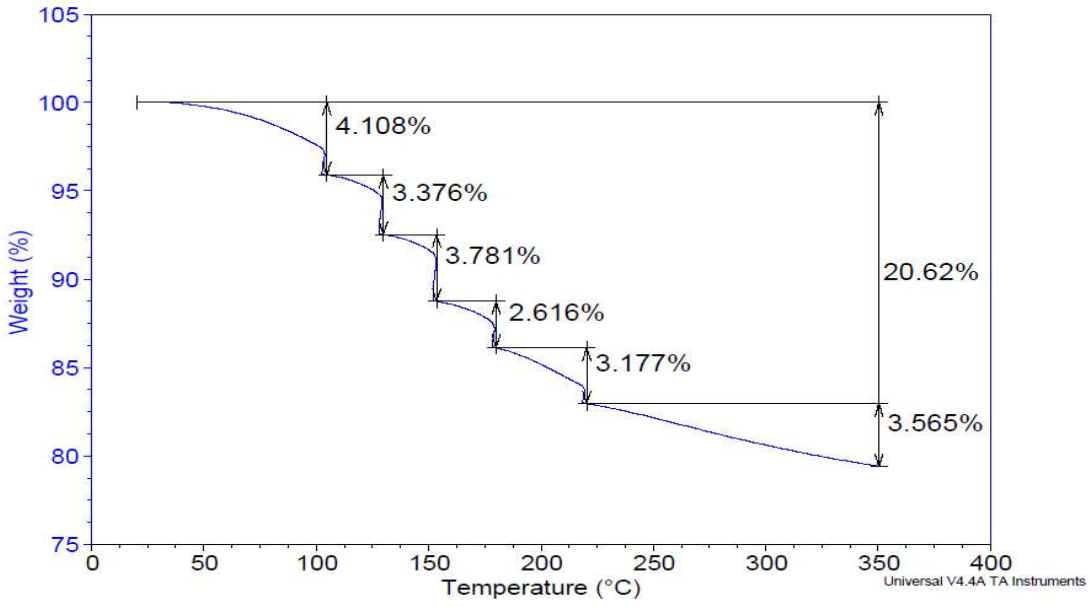

Figure 1.5 TGA plot of ZnO (0.05 M TBAB).

ZnO was also analyzed via TGA with two different concentrations of the surfactant, TBAB. The lower concentration (Figure 1.5) lost 21% mass by 350 ºC, but showed no particularly large isothermal losses, all of which were between 3% and 4% and distributed about every 25 ºC throughout from 100 ºC to about 225 ºC. The last drop, while still between 3% and 4%, occurred over a longer temperature range, from 225-350 ºC. At normal concentrations of TBAB (Figure 1.4), only 14% mass was lost, with a sharp drop from 100-125 ºC and a more gradual slope from 125-350 ºC. Evidently, the concentration of TBAB required by the procedure exhibits a lower mass loss than the lower concentration. It may be that the lower concentration of surfactant leads to a more exposed ZnO nanoparticle surface, which allows more of the oxygen to escape as temperature rises. It may also be that the lower concentration ZnO sample had not been completely purified, leaving free TBAB to vaporize during the analysis.

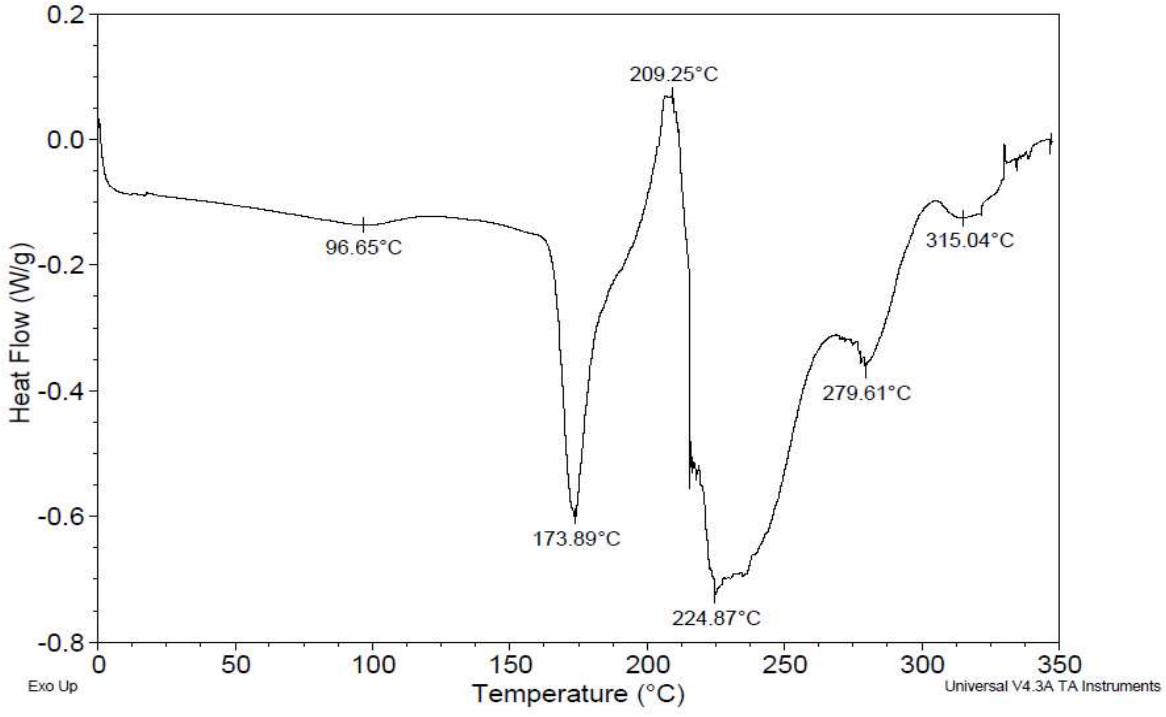

Figure 1.6 DSC plot of cyanine dye.

The DSC plot for cyanine dye shows four peaks of negative heat flow, and one positive peak. The first peak, which was the most shallow at -0.1363 W/g, occurred at 97 ºC. The second most negative peak occurred next, at -0.5998 W/g at 174 ºC. The only positive peak occurred at 209 ºC, with a magnitude of 0.06969 W/g. The most negative peak occurred at 225 ºC, with a magnitude of -0.7248, and the next two peaks, 280 ºC and 315 ºC, were increasingly less negative, with magnitudes of -0.3674 and -0.1253 W/g, respectively. As shown, the thermal breakdown of the dye is mostly exothermic, with a single endothermic peak. The conjugated aromatic rings are highly stable, and likely require a larger input of energy to break down than other sections of the dye.

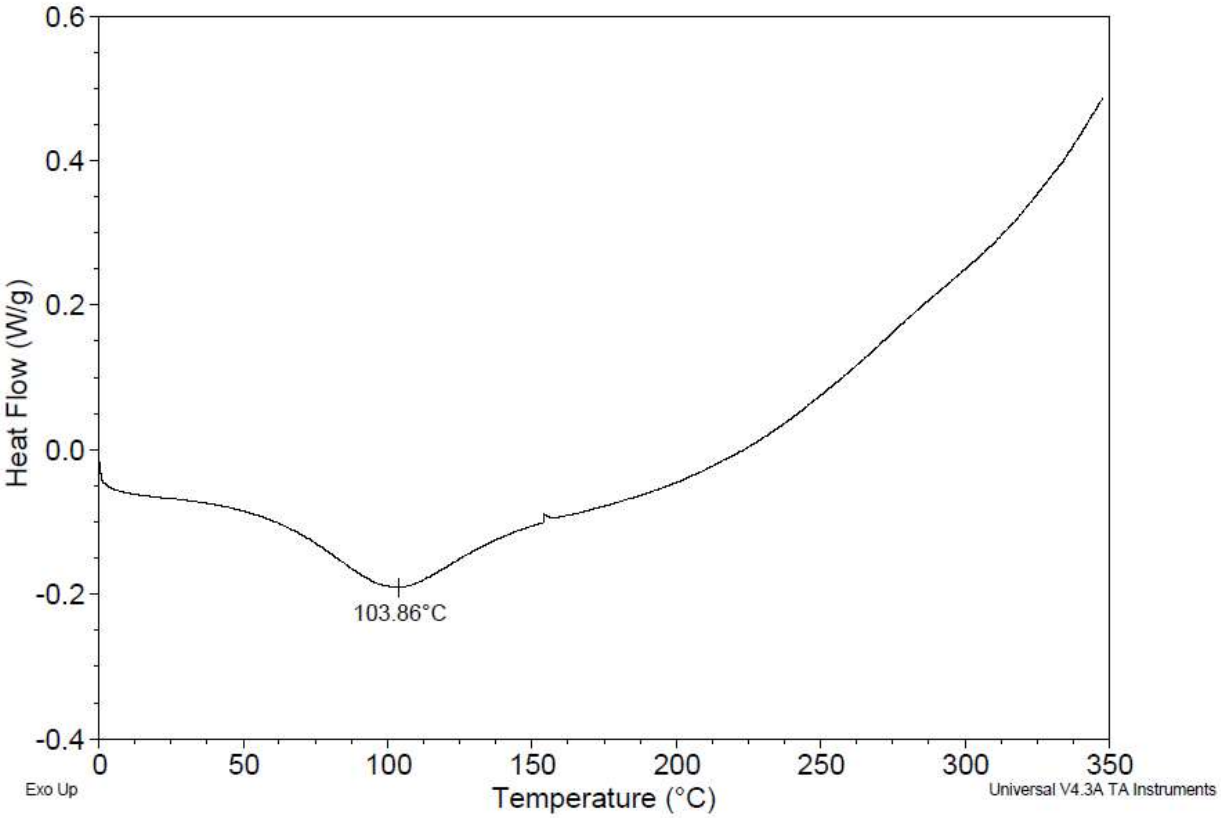

Figure 1.7 DSC plot of cyanine dye nanomaterial (0.1 mM dye).

The dye nanomaterial exhibited a single negative peak, -0.1908 W/g at 104 ºC. This is an ideal result, as the single exothermic peak corresponds to the solvent (MeOH) and not the dye itself, as shown through a comparison of Figures 1.7 and 1.8. The dye nanomaterial appears to retain complete thermal stability throughout the analysis.

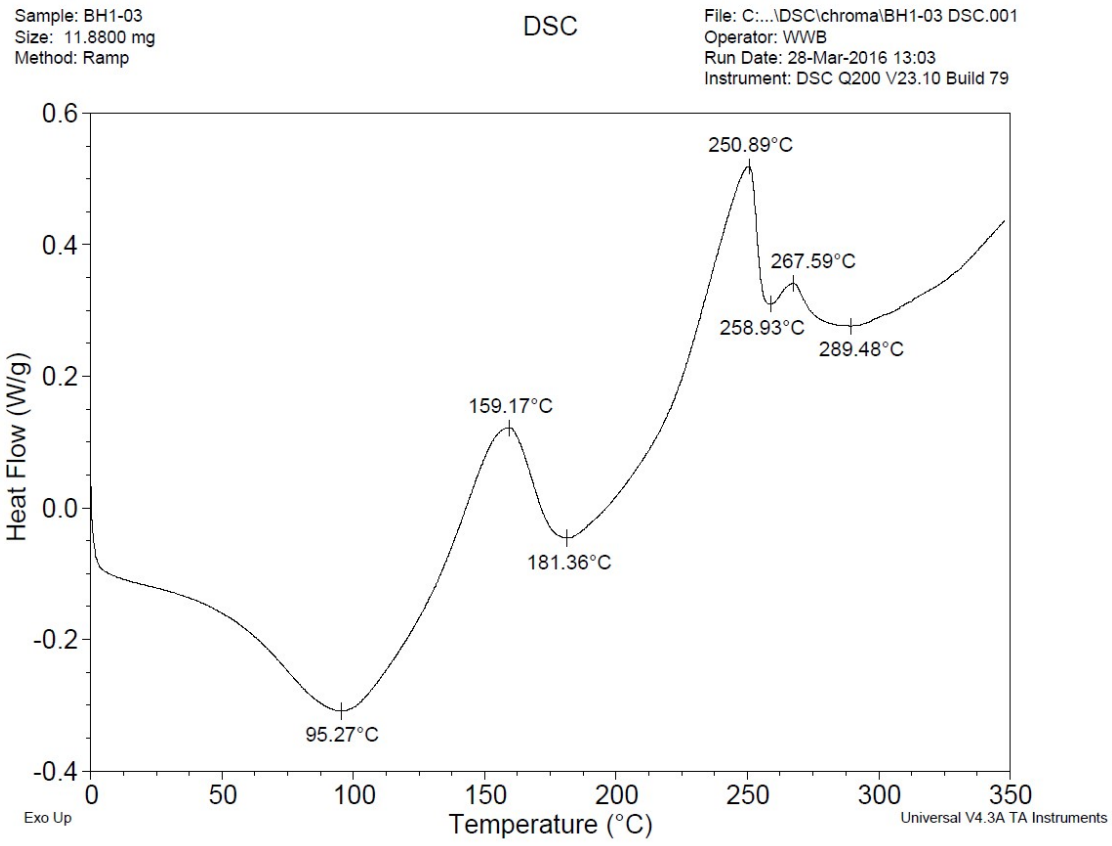

Figure 1.8 DSC plot of 1.0 mM dye nanomaterial.

The features in Figure 1.8 were not present in the 0.1 mM dye nanomaterial, and most likely due to the full concentration of dye used in the synthesis of the batch with 1.0 mM dye. The first exothermic peak at 95 ºC is likely to be the solvent used to purify the nanomaterial (MeOH), as it is also present in 0.1 mM dye and pure ZnO nanoparticles. The second exothermic peak at 181 ºC matches one of the exothermic reactions of the

dye, indicating that dye on the surface of the nanoparticles at full concentration is susceptible to reaction. The peak at 289 ºC also matches the dye, indicating the other peaks most likely belong to pure TBAB.

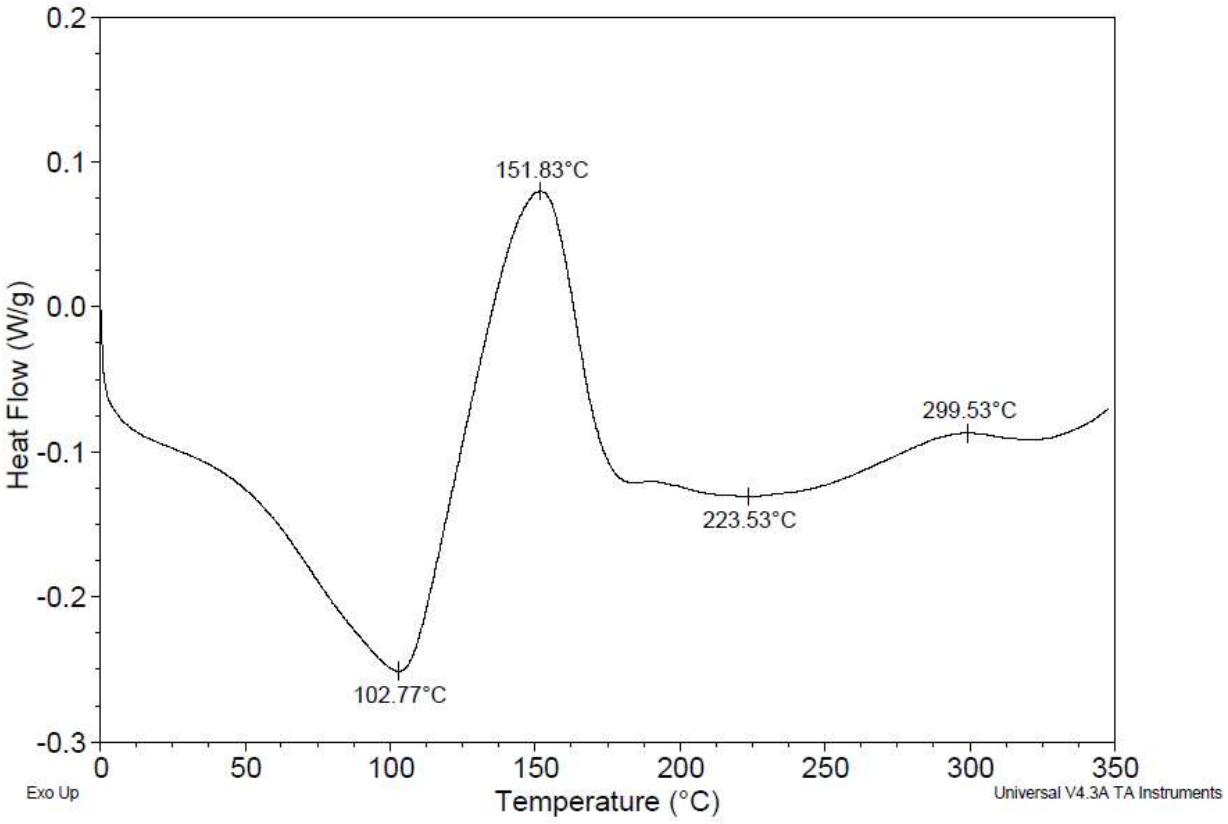

Figure 1.9 DSC plot of ZnO nanoparticles (0.1 M TBAB).

Pure ZnO nanoparticles exhibited a similar exothermic peak of -0.2513 W/g at 103 ºC, but also showed an endotherm at 152 ºC and two more exothermic peaks at 224 ºC and 299.53 ºC, with magnitudes of .07967 W/g, -0.1309 W/g, and -0.0871 W/g, respectively. While the identity of the endothermic and last two exothermic peaks remains unknown, what is important is that the first exothermic peak matches that of the single peak in Figure 1.7, indicating that the heat loss came from the evaporation of the solvent, and not from the dye itself. Since the goal of this project is to stabilize the dye without interfering

with its absorbance, the DSC and TGA plots indicate success as far as thermal stabilization is concerned.

3.2. **Scanning Electron Microscopy (SEM)**

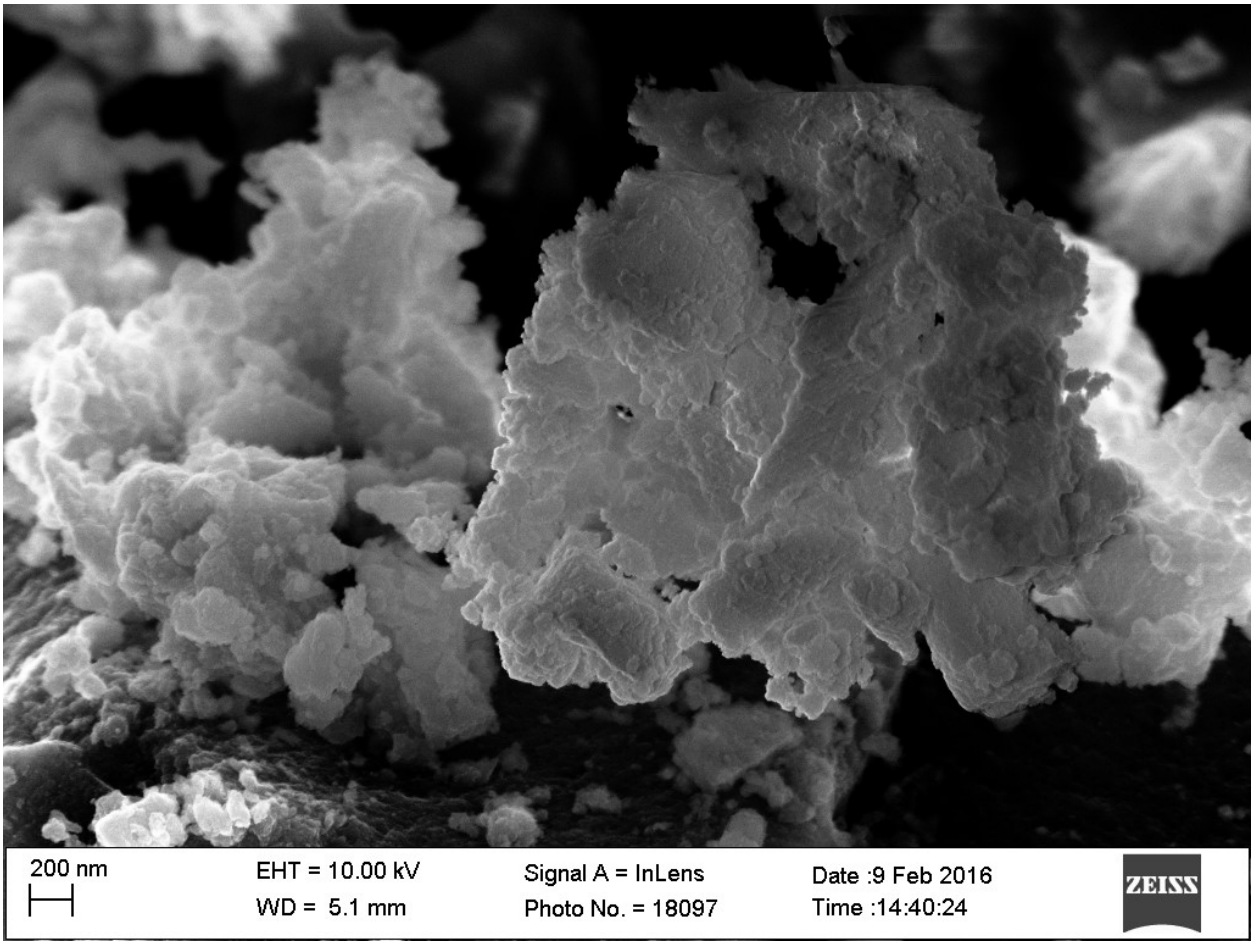

Figure 2.1 SEM image of aggregated nanomaterial (0.1 mM dye).

Figure 2.1 shows that the nanomaterial had a high level of aggregation when prepared through the normal synthetic method. This is likely due to the large amounts of organic molecules, like TBAB and the dye itself, aggregating in the absence of solvent.

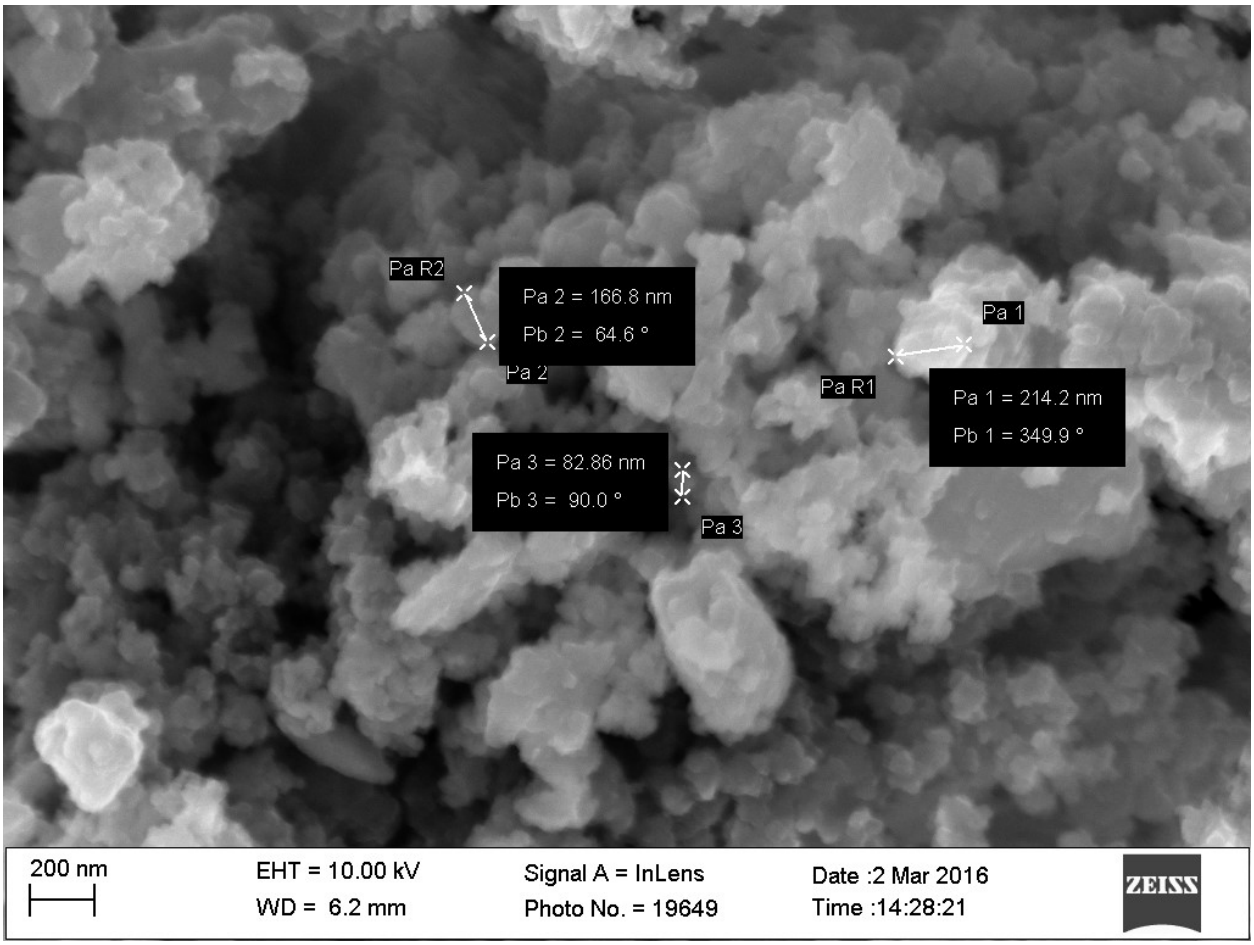

Figure 2.2 SEM image of individual nanomaterial particles (0.1 mM dye).

On closer inspection, Figure 2.2 reveals the average nanoparticle size is ~150 nm. The dye itself was difficult to image due to its lack of conductivity, but the ZnO nanoparticle component showed up with relatively high resolution after carbon coating. Though aggregated, these particles can be seen as discrete chunks of ZnO, and their size can be estimated using the scale bar and diameter measurement features of the SEM. The average particle size was found to be 94 nm ± 39 nm.

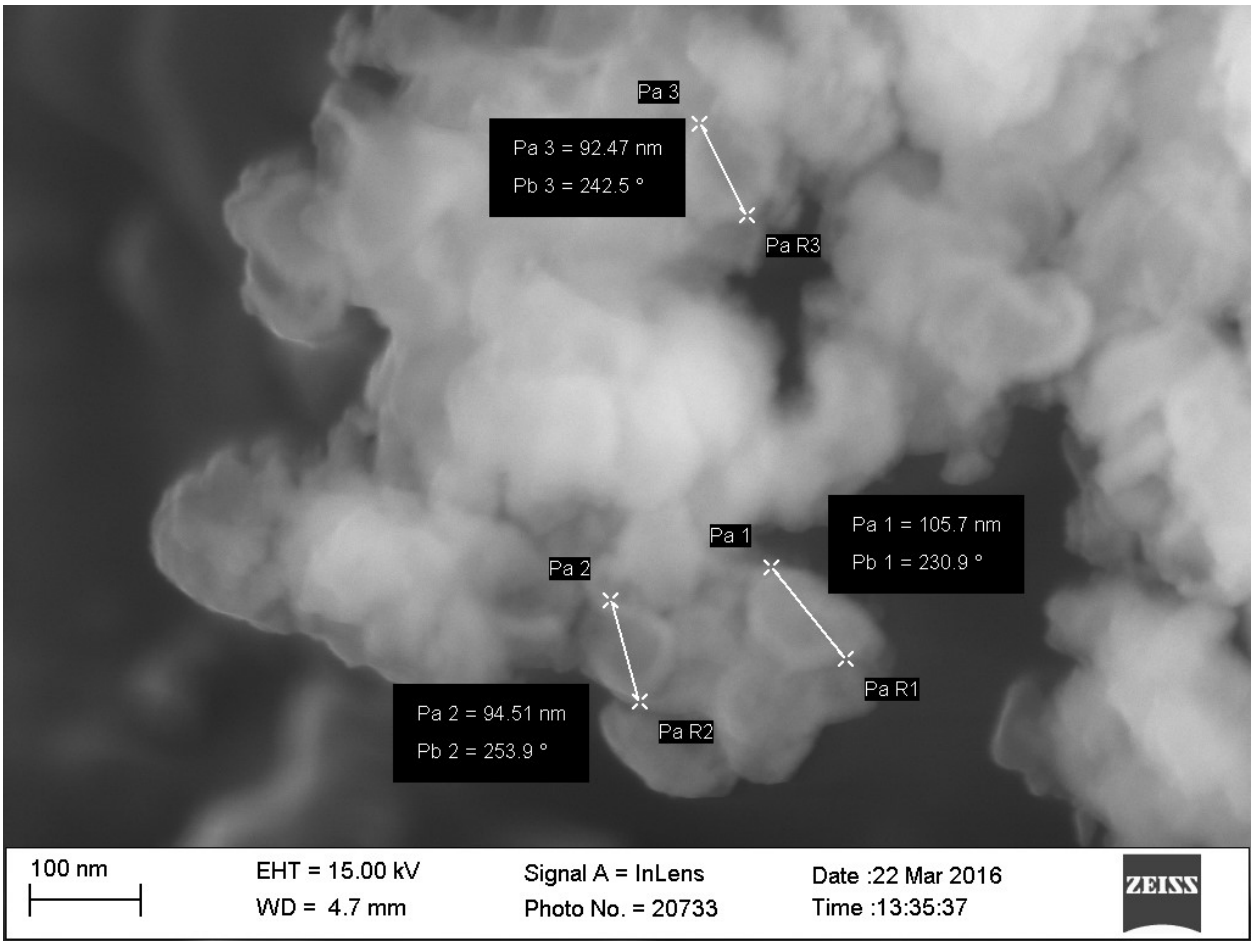

Figure 2.3 SEM image of individual nanomaterial particles (1.0 mM dye).

Owing to the fact that the batch with 1.0 mM dye contained more dye, and also that stirring was introduced with this synthesis, the particle size is smaller and more regular than the batch with 0.1 mM dye. Pictured in Figure 2.3, the average particle size was 102 nm, ± 20 nm. This is a better outcome than was found with the batch with 0.1 mM dye, showing a more controlled particle size and retaining the proper spectrophotometric characteristics, as described in Sections 3.6 and 3.8.

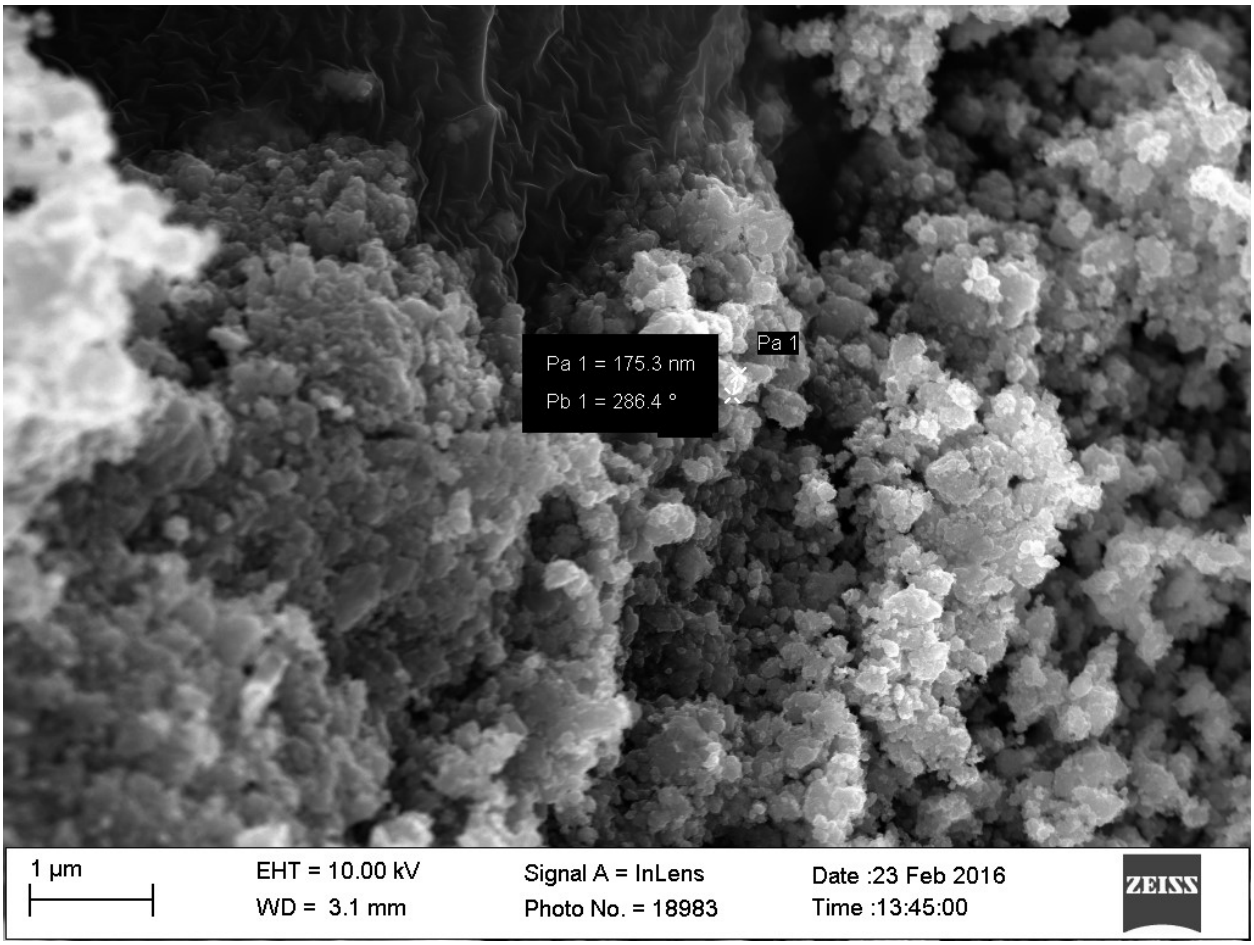

Figure 2.4 SEM image of ZnO powder (0.1 M).

When varying the amount of TBAB, nanoparticle ZnO (without dye) was imaged at three different synthesis concentrations: 0.1, 0.05, and 0.5 M. At normal concentrations (0.1 M), there was an average to low amount of aggregation, with particle sizes ranging from 150 to 400 nm. The absence of dye appears to have lowered the degree of aggregation, suggesting that it may play an active role in the aggregation.

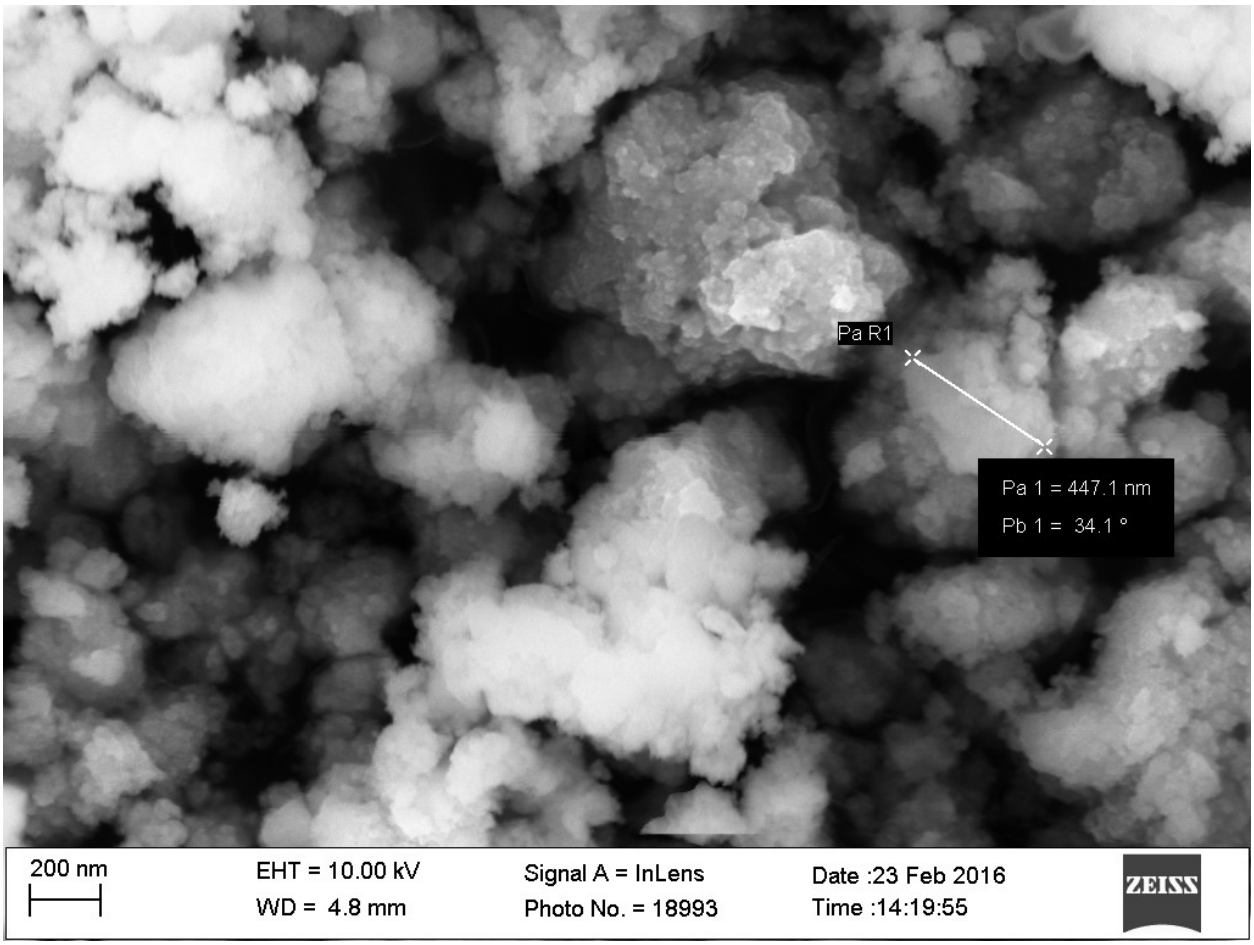

Figure 2.5 SEM image of ZnO powder (0.05 M).

The lower concentration, 0.05 M, resulted in larger particle sizes around 200-450 nm. It appears that lower concentrations of TBAB encourage the particles of ZnO grow larger, as there is less surfactant to restrict access their surface of the growing moiety.

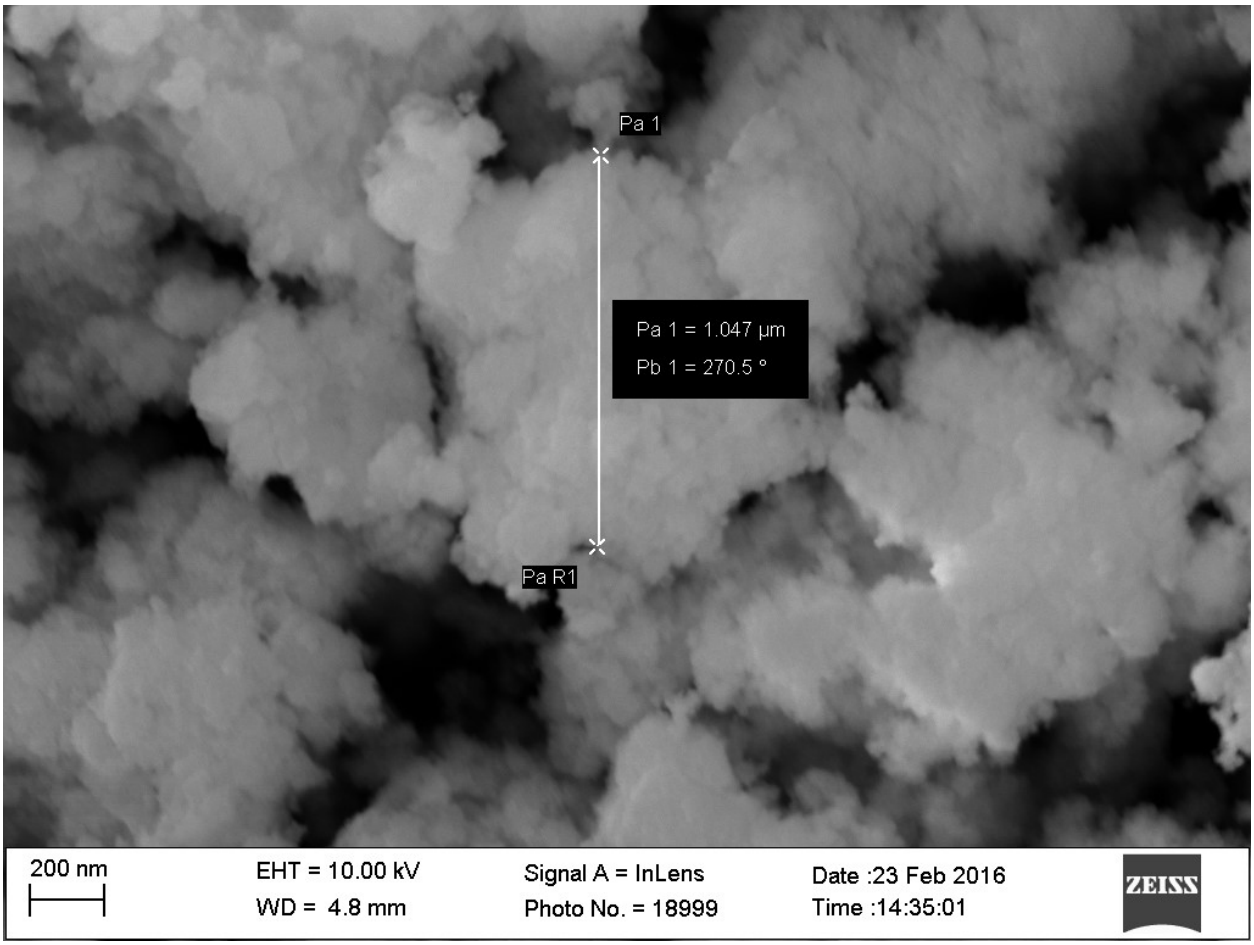

Figure 2.6 SEM image of ZnO-TBAB crystals (0.5 M).

The highest concentration (0.5 M) tested may not have been properly cleaned of excess TBAB, as it was significantly more crystalline and less powdery. The aggregation was significantly worse, resulting in particles approximately 650 to 1000 nm. With further cleaning, it is possible that these particles would be smaller than the lower concentrations of TBAB, due to the surfactant occupying surface sites of the ZnO.

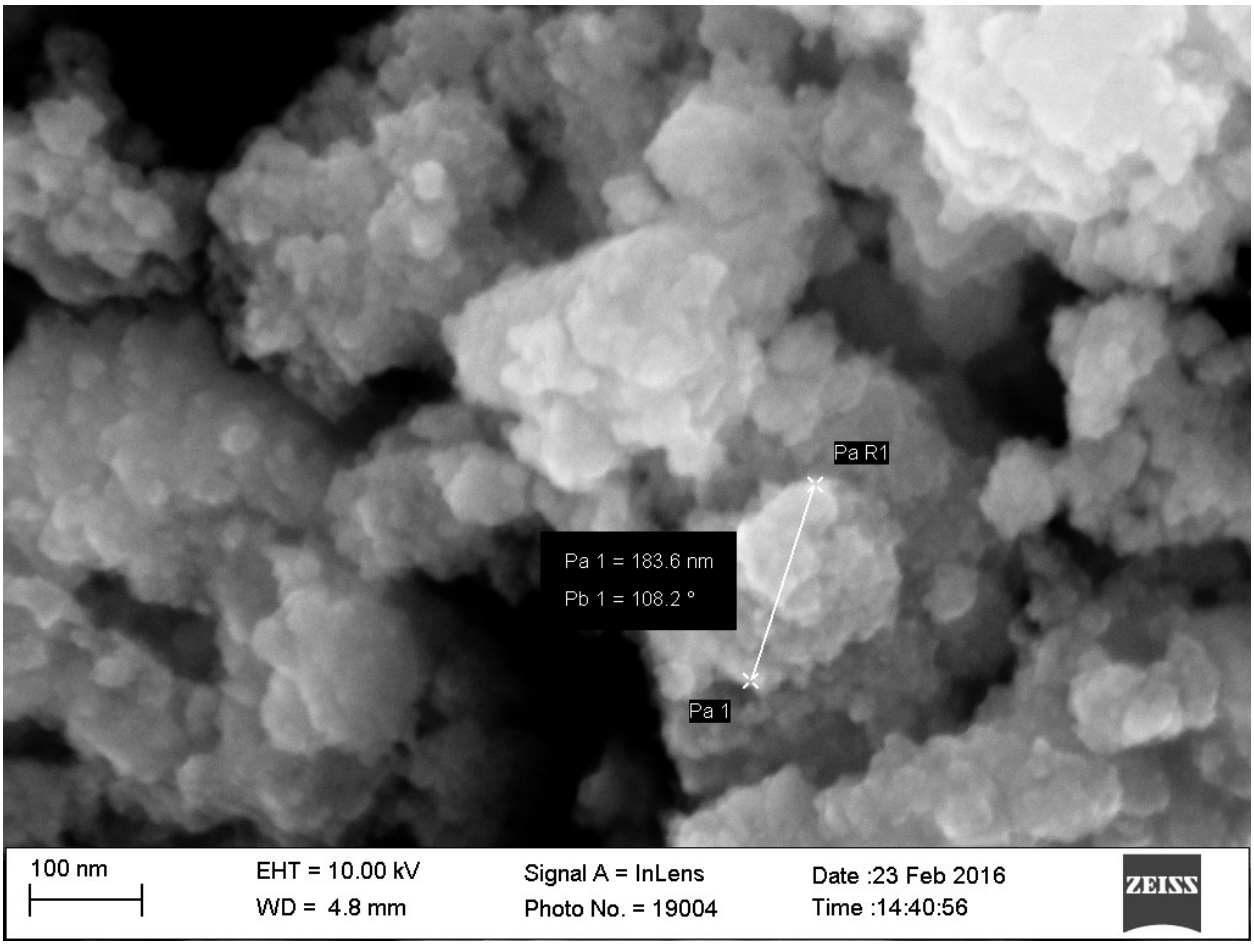

Figure 2.7 SEM image of individual ZnO particles (0.5 M).

When examined closely, the average size of the less aggregated clusters was between 180 and 200 nm. It is clear that the particles themselves are even smaller, possibly between 10-50 nm in size, but the degree of aggregation renders this quality useless with regards to this project. With an excess of aggregation, shifts in the absorbance spectrum will appear and alter the visible properties of the dye, which is what this project is intended to avoid.

3.3. **Transmission Electron Microscopy (TEM)**

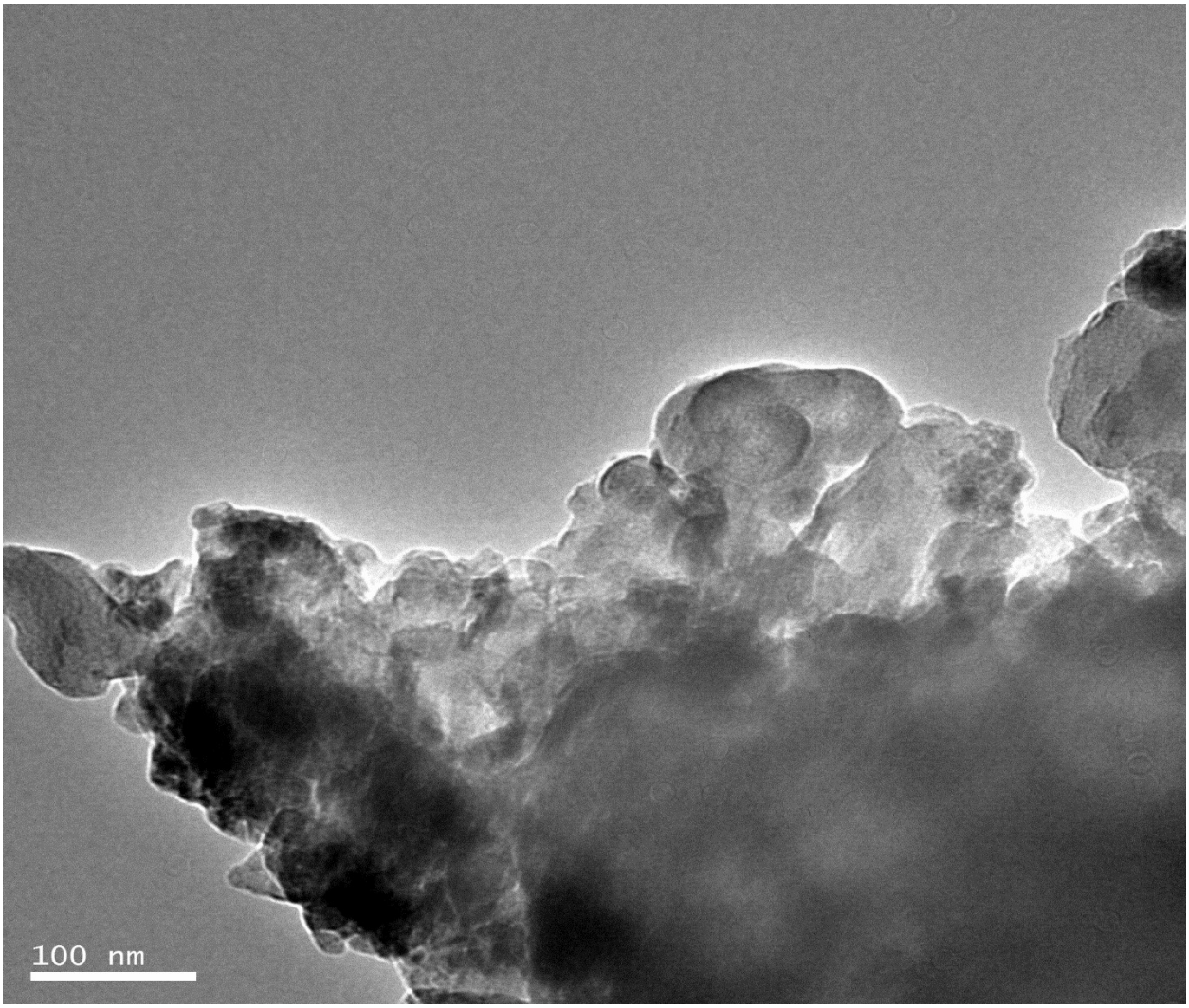

Figure 3.1 TEM image of 0.1 mM dye nanomaterial.

When attempting to image 0.1 mM dye, it was found that the nanomaterial was too aggregated to image individual nanoparticles satisfactorily. Most of the images recorded by TEM were unable to penetrate the layers of nanomaterial, and were uninformative. As is visible in one of the only usable images, Figure 3.1, the particles are around to 100 nm in size, and are heavily aggregated.

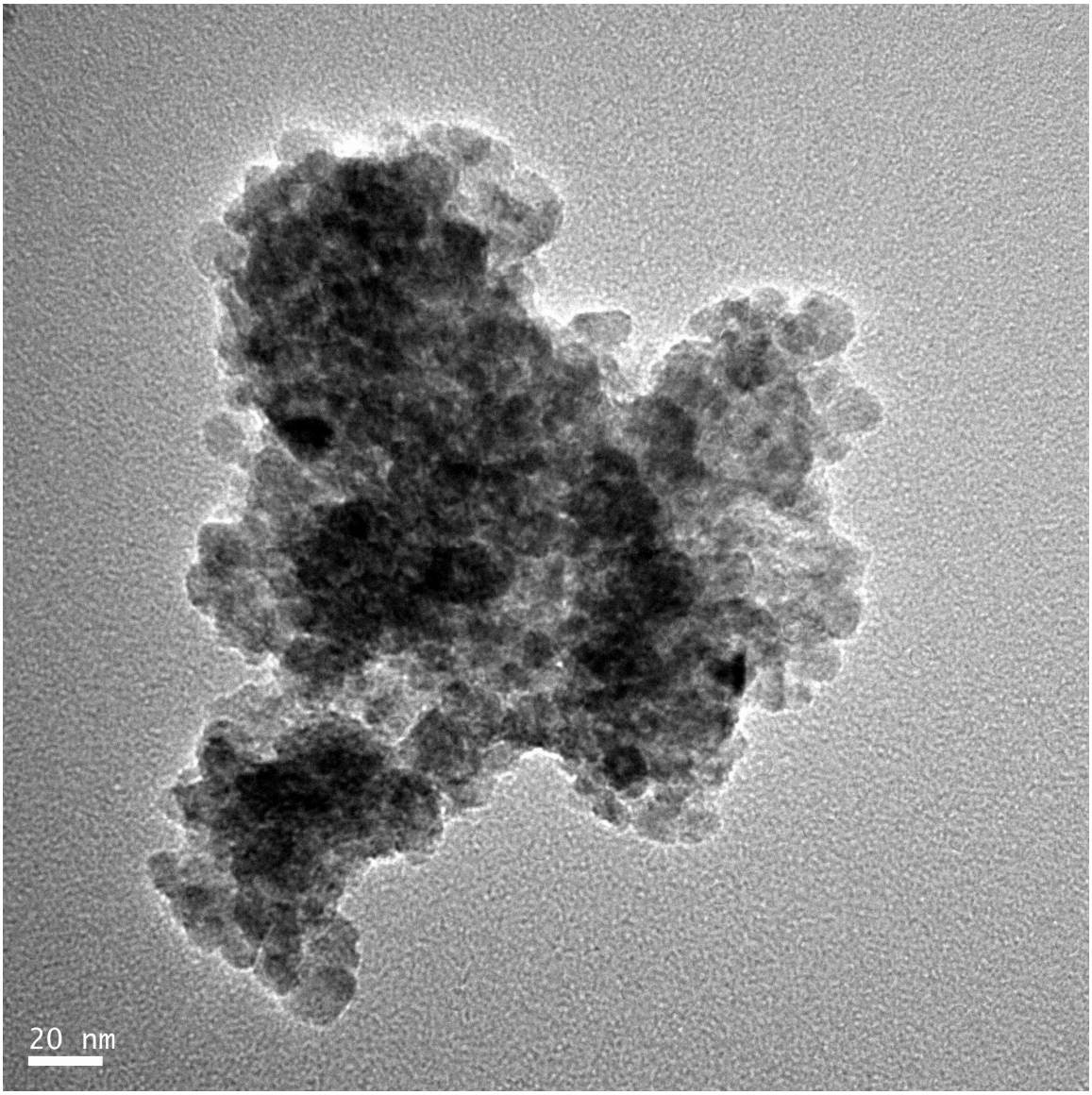

Figure 3.2 TEM image of 1.0 mM dye nanomaterial.

1.0 mM dye proved to be both less aggregated and smaller in particle size than 0.1 mM dye, likely due to the addition of more dye binding to the surface and to the use of stirring. Individual particles appear to be 20 nm or smaller, albeit heavily aggregated.

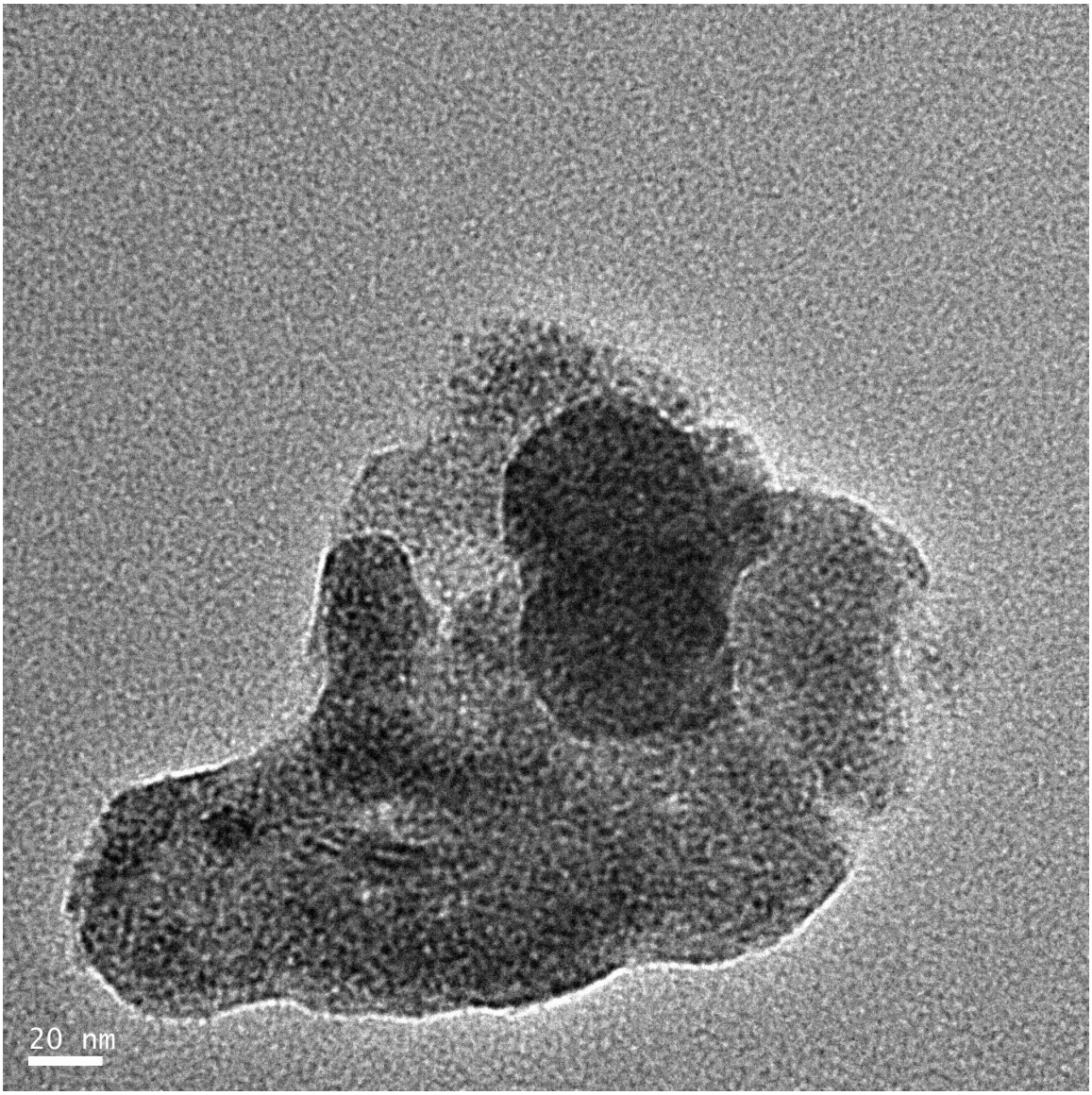

Figure 3.3 TEM image of 1.0 mM dye nanomaterial aggregate

After isolating one particularly small aggregate of the 1.0 mM dye material, it is difficult to distinguish between aggregated chunks and individual particles. From what is observed, it appears that the particles in Figure 933 are roughly 40-60 nm in size, which represents an improvement over 0.1 mM dye.

3.4. **Raman Spectroscopy**

Assuming that the dye remains unperturbed after bonding with ZnO for all parts but the COO^- linker, Raman spectroscopy should not show significant differences between cyanine dye and the cyanine dye nanomaterial. Figure 4.1 presents the spectra measured for the dye, nanomaterial, ZnO, and TBAB.

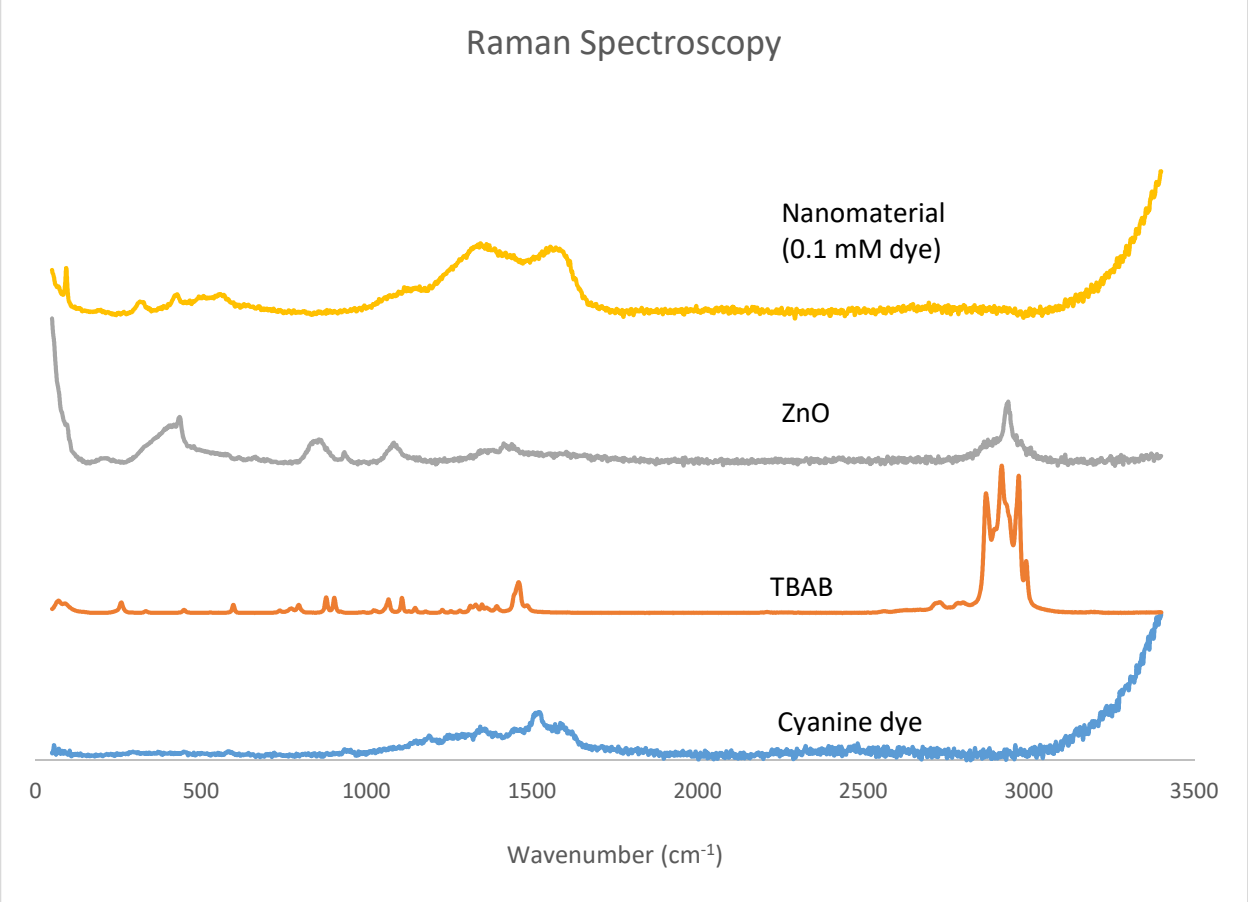

Figure 4.1 Raman spectra of nanomaterial 0.1 mM dye and its constituents.

As depicted in Figure 4.1, the ZnO generated in the absence of cyanine dye still exhibits peaks for TBAB high-frequency C-H vibrational modes (2870-2990 cm^{-1}), indicating that the surfactant adhered to the surface after purification. However, the nanomaterial shows

no such TBAB C-H peaks, implying that the dye displaced the TBAB from the surface of the nanoparticles, allowing it to be removed entirely. Additionally, the characteristic peak of the dye appears within the nanomaterial, albeit with a slightly different form. This could be due to the fact that the dye continually degraded during laser exposure, causing it to lose its characteristic peaks. It could also be that the double-peak exhibited at 1360 and 1580 cm^{-1} in the nanomaterial is the true Raman characteristic vibrational response of the dye, without thermal degradation. Regardless, the dye is expected to exhibit C=C stretching and CH_2 rocking vibrational modes at the highest intensity, given its high degree of conjugation and its long aliphatic chains, respectively. Given that the twin peaks of the nanomaterial, 1370 and 1590 cm^{-1}, occur at frequencies consistent with CH_2 rocking and C=C stretching (respectively), it is likely that the nanomaterial preserved the dye's Raman spectrum without significant alterations.

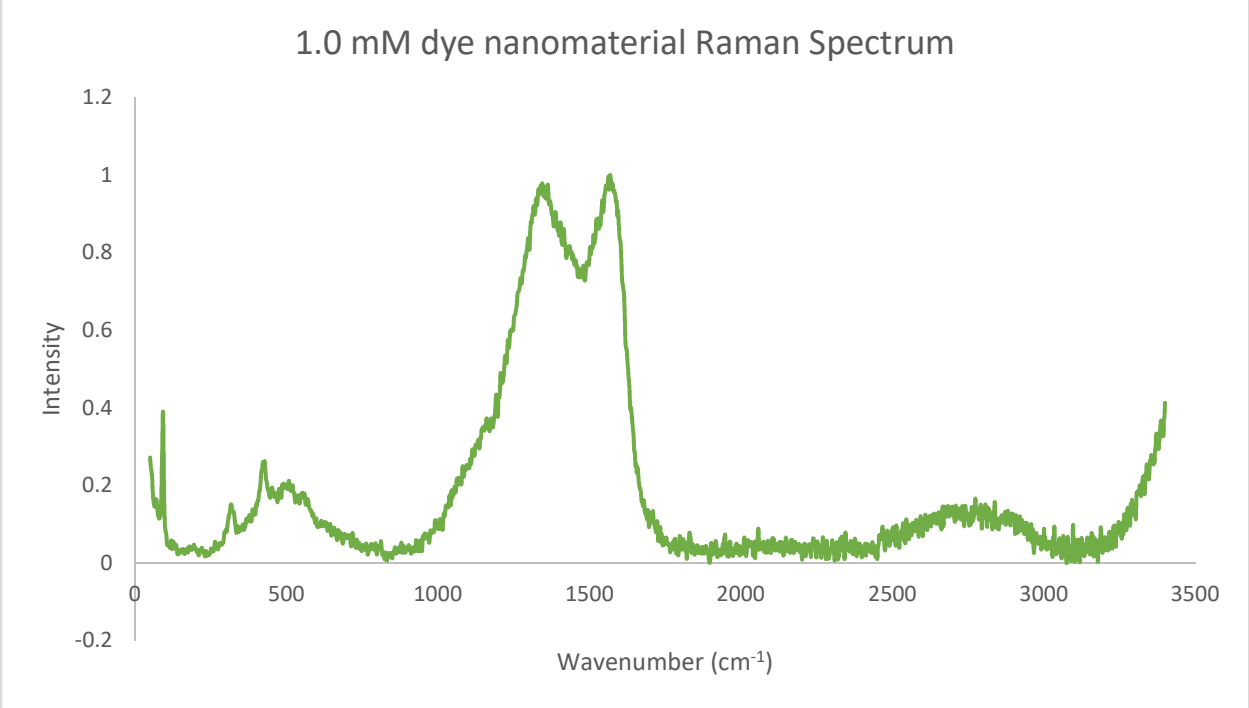

Figure 4.2 Raman spectrum of 1.0 mM dye nanomaterial.

1.0 mM dye appears to share the same double-peak as 0.1 mM dye, although with significantly greater intensity. This appears to be a shared characteristic with the pure dye, although the dye peaks are degraded due to the nature of the measurement. The other peaks all belong to pure ZnO and TBAB. The feature between 2500 – 3000 cm^{-1} is fairly broad and unresolved, but is most likely correlated with TBAB. Judging from the previous Raman spectra, there is no other provenance apart from TBAB, implying that this sample of nanoparticles was not completely purified of TBAB before analysis.

3.5. **Energy-Dispersive X-ray Spectroscopy (EDX)**

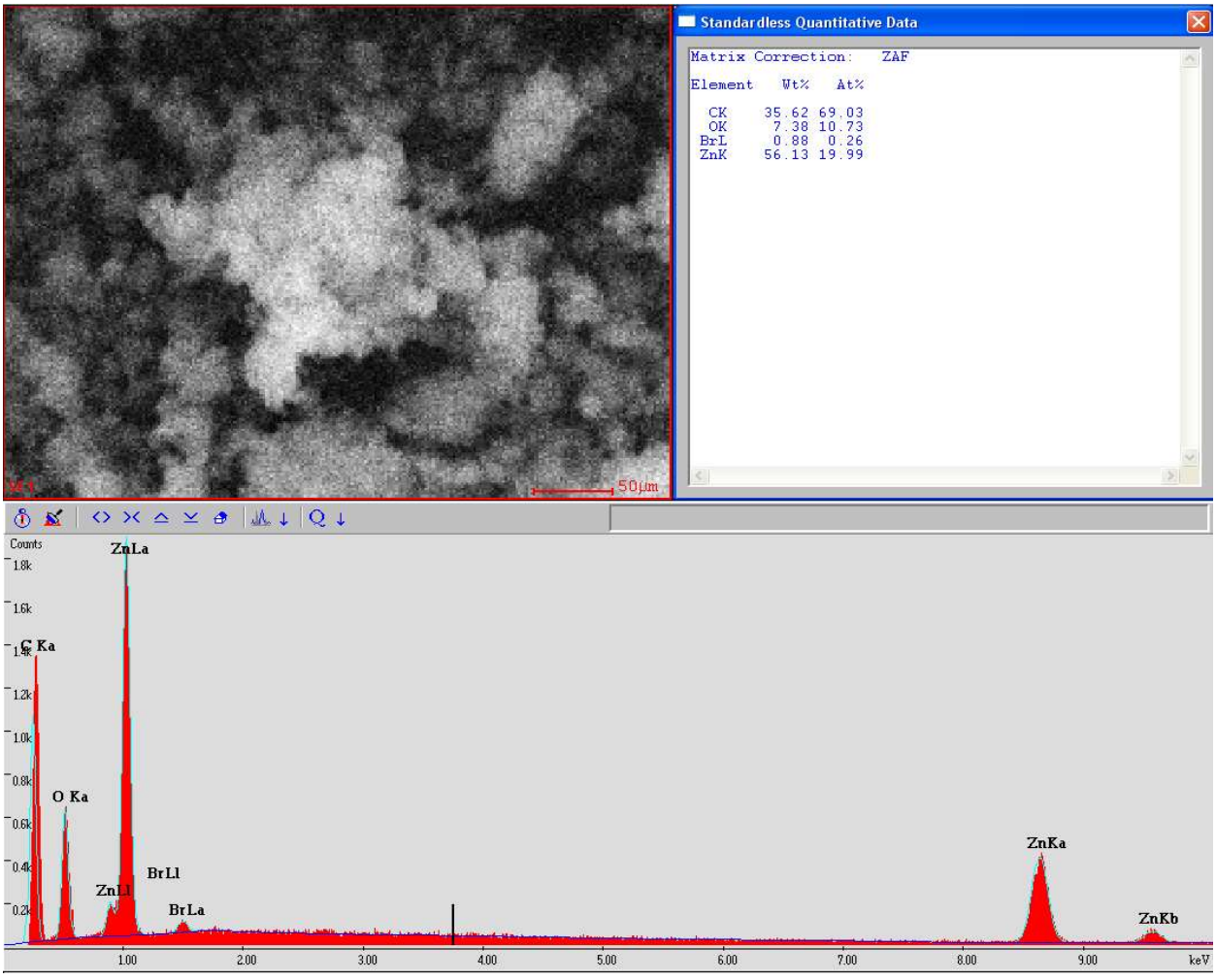

Figure 5.1 EDX plot of ZnO nanoparticles.

The characteristic peaks exhibited in the EDX plot of ZnO are exactly as expected. All four characteristic zinc peaks appear, as well as two bromine peaks due to the presence of TBAB. Carbon and oxygen are present in this analysis, as in every other. Bromine is only present in trace quantities, with the major constituents being carbon and zinc. Unexpectedly, zinc had twice the atomic percent composition of oxygen, even though it is expected oxygen would at least equal zinc due to the one-to-one molar ratio of ZnO. While this result is unexpected, as long as the optical properties of the dye are unaffected while still achieving thermal stabilization, it doesn't have a large influence on this project's success.

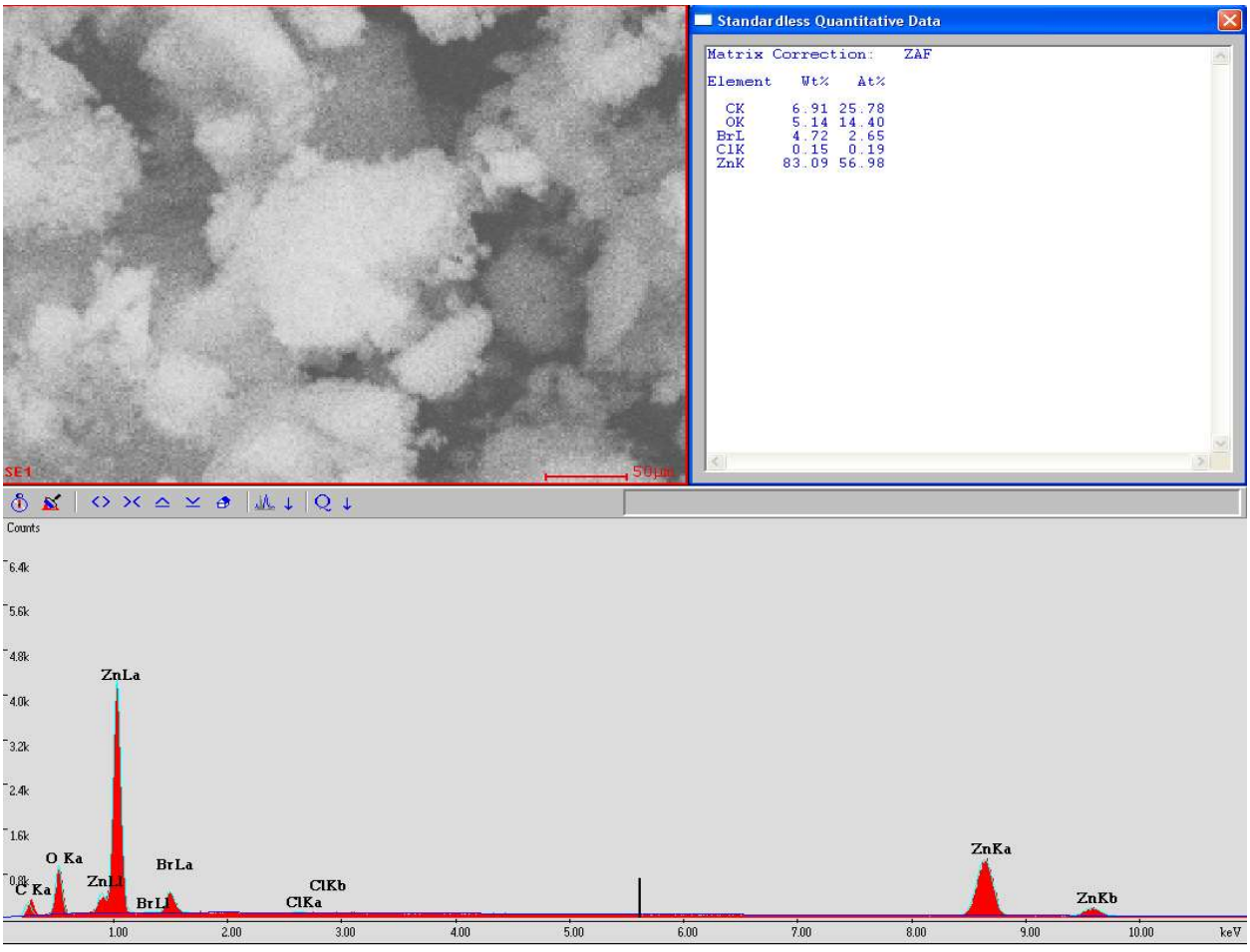

Figure 5.2 EDX plot of nanomaterial (0.1 mM dye).

When the nanomaterial was examined, zinc was the most abundant constituent, even outstripping carbon. Bromide was still present, however, chloride had been introduced, being the counter-ion of cyanine dye. This nanomaterial was made with a less concentrated dye solution, which is likely the reason for the domination of the zinc. Figure 5.2 will be compared with Figure 5.3.

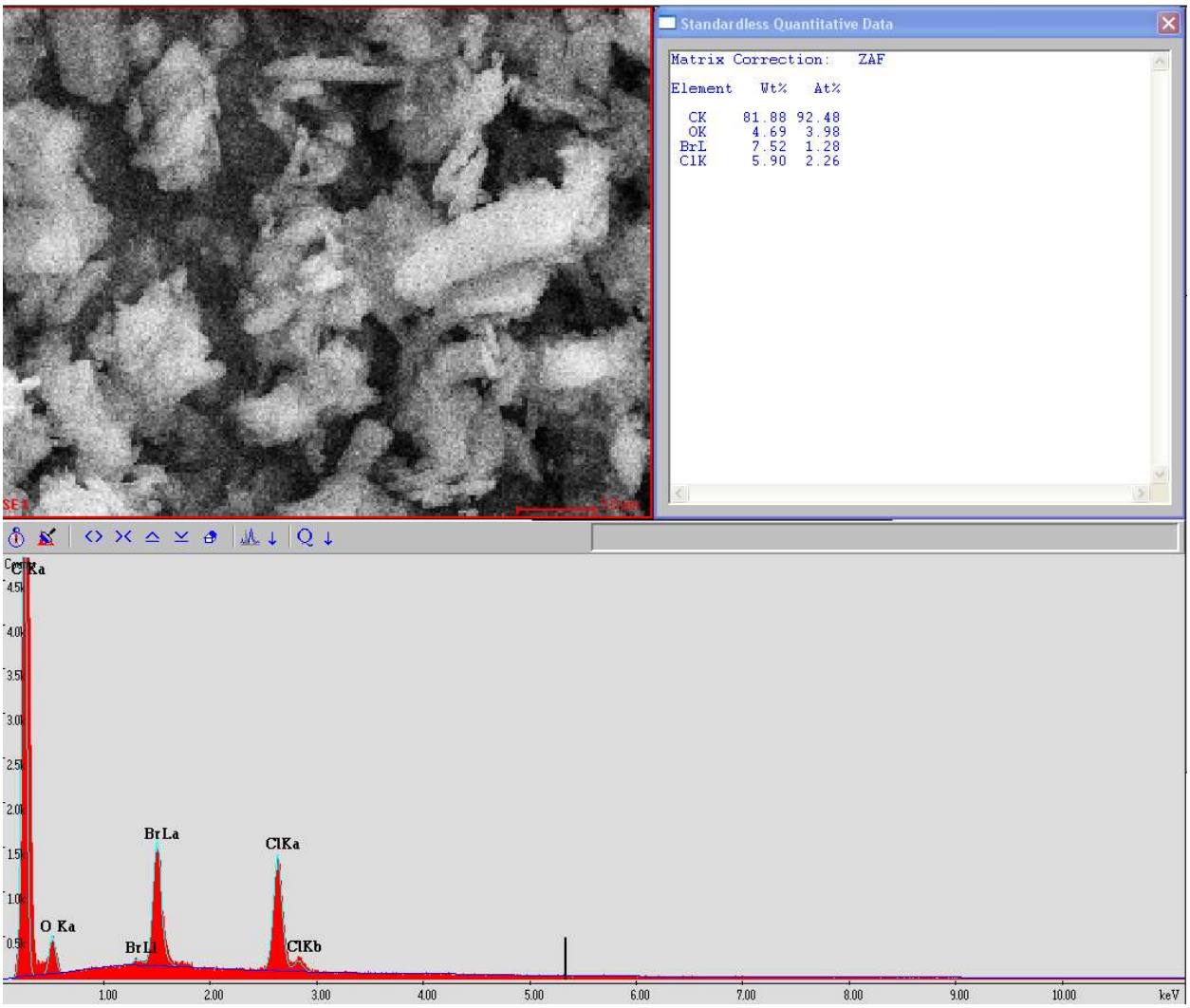

Figure 5.3 EDX plot of cyanine dye.

As expected, the major constituent of the dye is carbon, with trace amounts of chlorine and oxygen. What is unexpected, however, is the presence of bromide in comparable

quantities to chloride. There is negligible chance that TBAB was introduced to this dye sample, as it was taken straight from the reagent bottle.

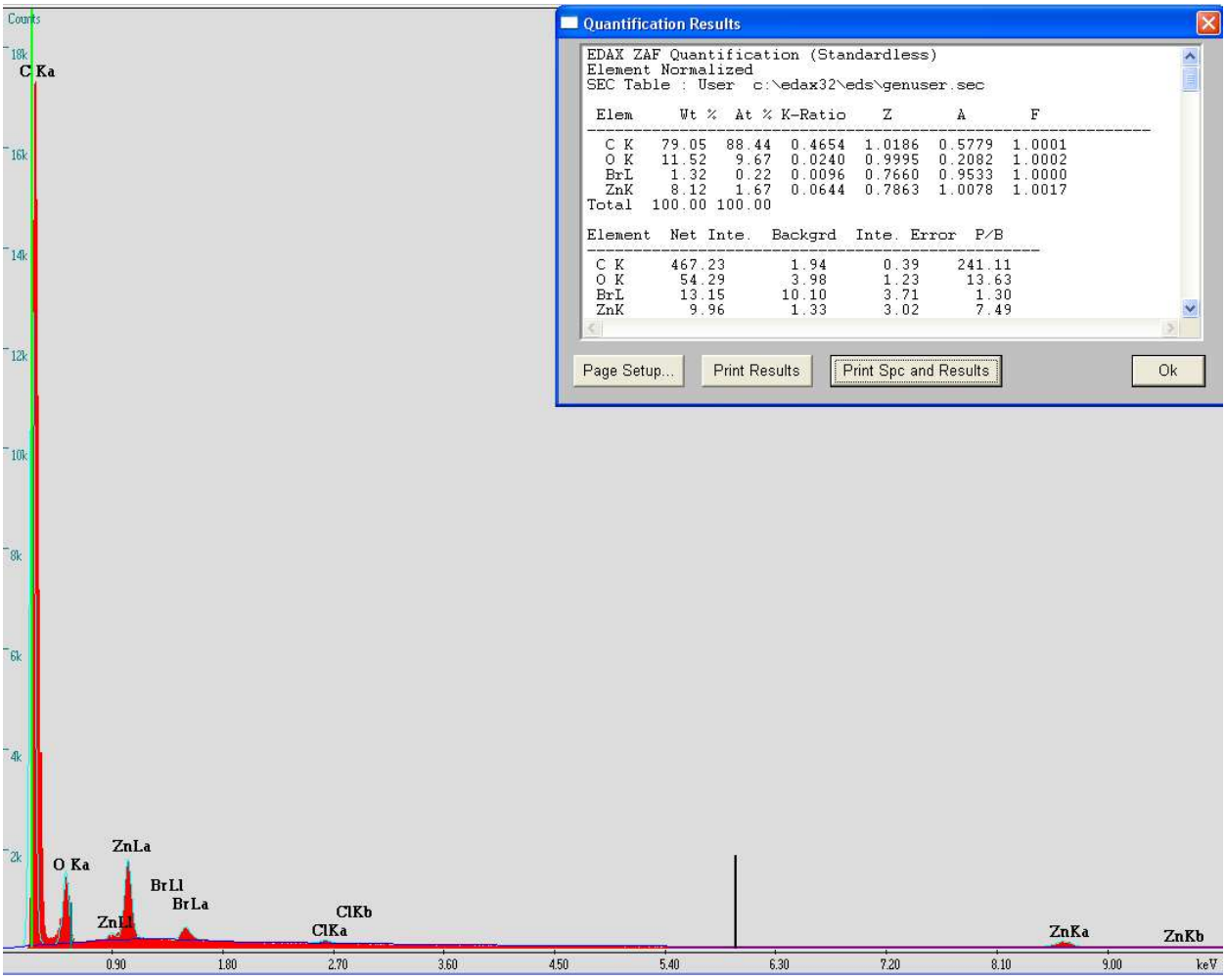

Figure 5.4 EDX analysis of the batch with 1.0 mM dye.

Given that 1.0 mM dye was prepared with the correct concentration of organic dye, the zinc peaks have been obscured by the significantly larger carbon peak. Not all of this carbon came from dye, but the fact that both samples 0.1 mM dye and 1.0 mM dye were carbon coated, yet 1.0 mM dye had a dominant carbon peak relates to the difference in concentration of organic dye. In each case, both the bromide and chloride peaks are still present, with marginally more of the former. This is either due to residual TBAB and dye

that could not be removed, or an indication that the nanoparticles should be purified more rigorously. In either case, these results indicate success in grafting the dye onto ZnO nanoparticle surfaces.

3.6. **Fluorimetry**

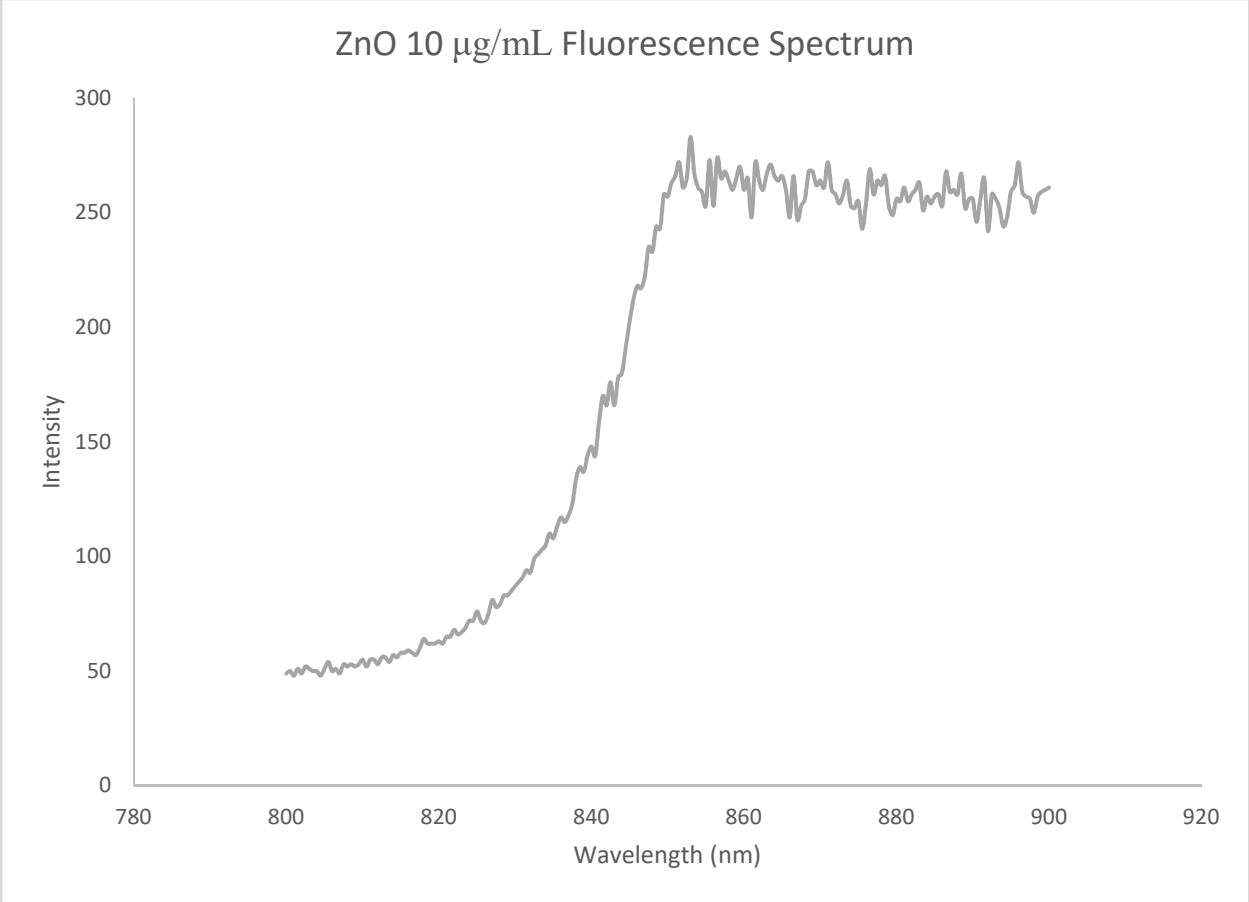

Figure 6.1 Fluorescence spectrum of ZnO nanoparticles.

As seen in the spectrum in Figure 6.1, ZnO is excited by the 532 nm light and steadily emits over a broad near-infrared range. This reaches plateau at around 855 nm, regardless of concentration of the nanoparticles. This phenomenon may cause an increase

in the nanomaterial fluorescence after 855 nm, but should not interfere with the emission peak exhibited in cyanine dye.

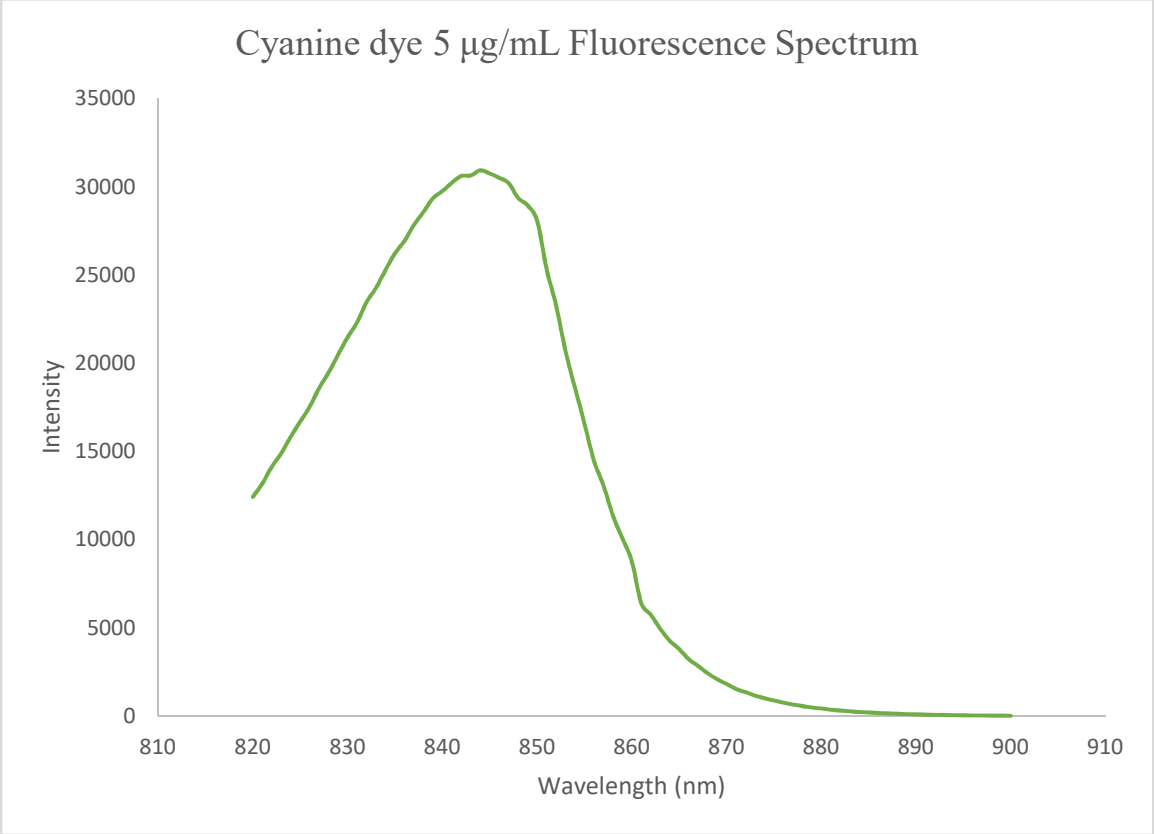

Figure 6.2 Fluorescence spectrum of cyanine dye.

This fluorescent spectrum of cyanine dye was measured with methanol solvent and an excitation wavelength of 820 nm. The maximum intensity feature occurs at 845 nm, 26 nm higher than the characteristic absorption peak of the dye. It is expected that the nanomaterial will retain this emissions maximum, with only a minor shift anticipated due to the binding to the ZnO and the increased ZnO fluorescence after 855 nm.

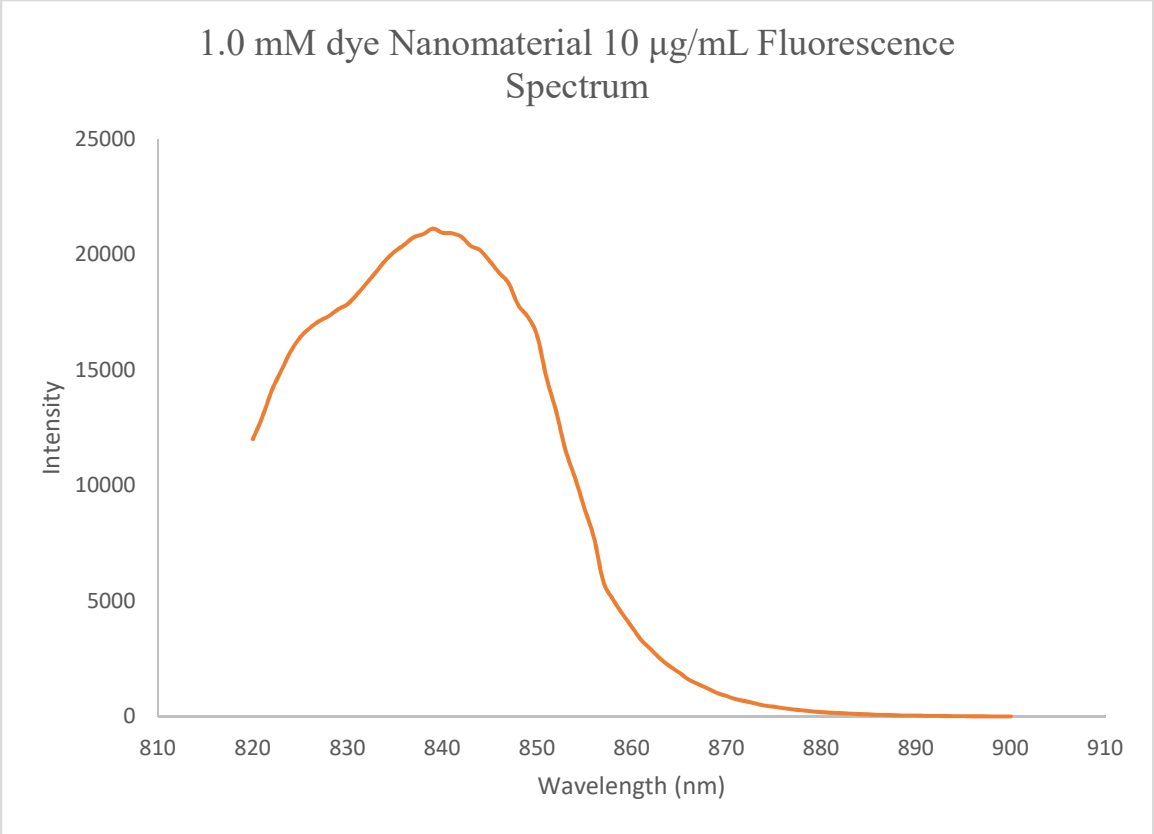

Figure 6.3 Fluorescence spectrum of 1.0 mM dye nanomaterial.

Imaged in Figure 6.3, the nanomaterial retained the same feature as cyanine dye, with an additional shoulder towards a blue shift. The main emissions peak occurs at 840 nm, shifted 5 nm from the dye fluorescent spectrum in Figure 6.2. These shifts are likely an effect of the addition of ZnO to the dye; ZnO's wide bandgap of 3.37 eV allows for higher-energy transitions to occur, resulting in a blue shift in the fluorescent spectrum. In future work, the bandgaps of cyanine dye, ZnO nanoparticles, and cyanine dye nanomaterial will be measured and compared.

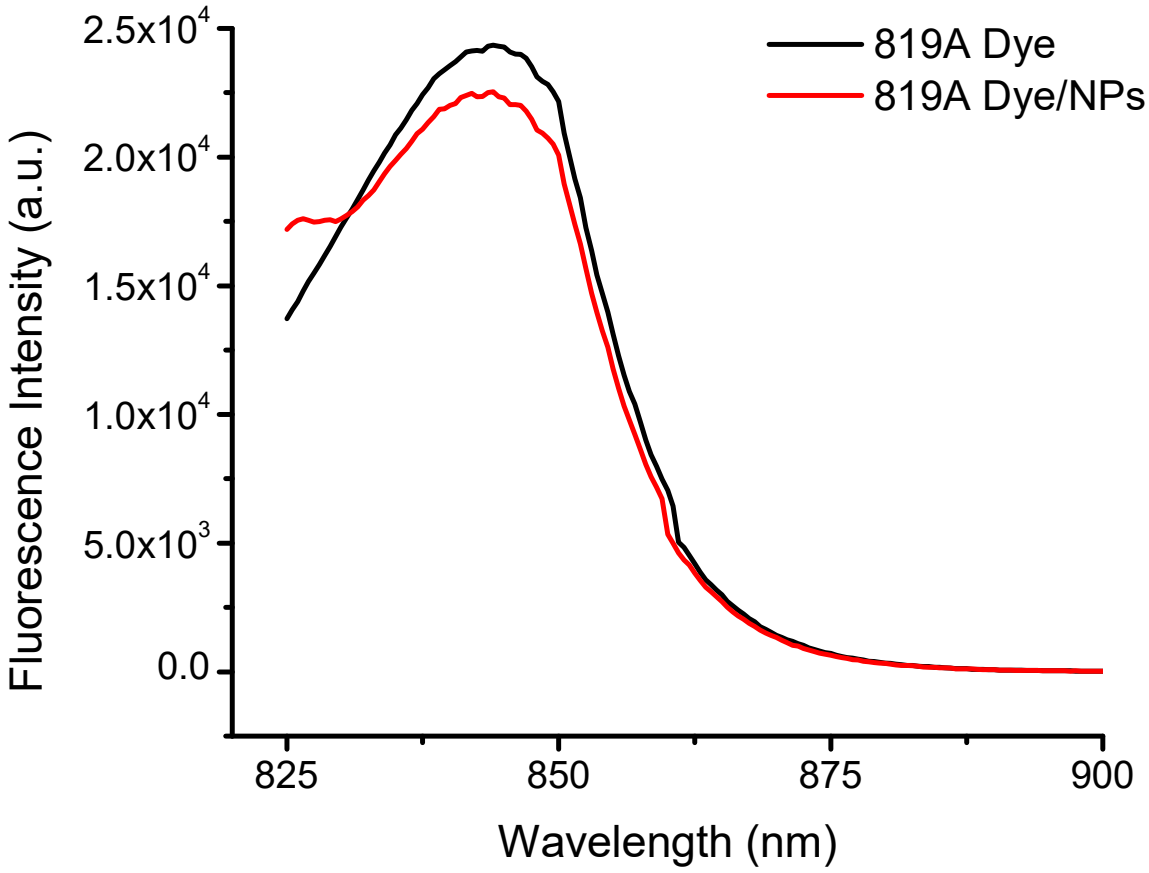

Figure 6.4 Fluorescence spectrum of cyanine dye and 1.0 mM dye nanomaterial

As is evident, the nanomaterial has nearly the same intensity of fluorescence as the pure dye without significantly shifting of the emission peak. It is clear that the process of nanomaterial generation, while drastically affecting the thermal stability, does not alter the optical properties of the dye to a significant degree.

3.7. **Fourier Transform Infrared Spectroscopy (FT-IR)**

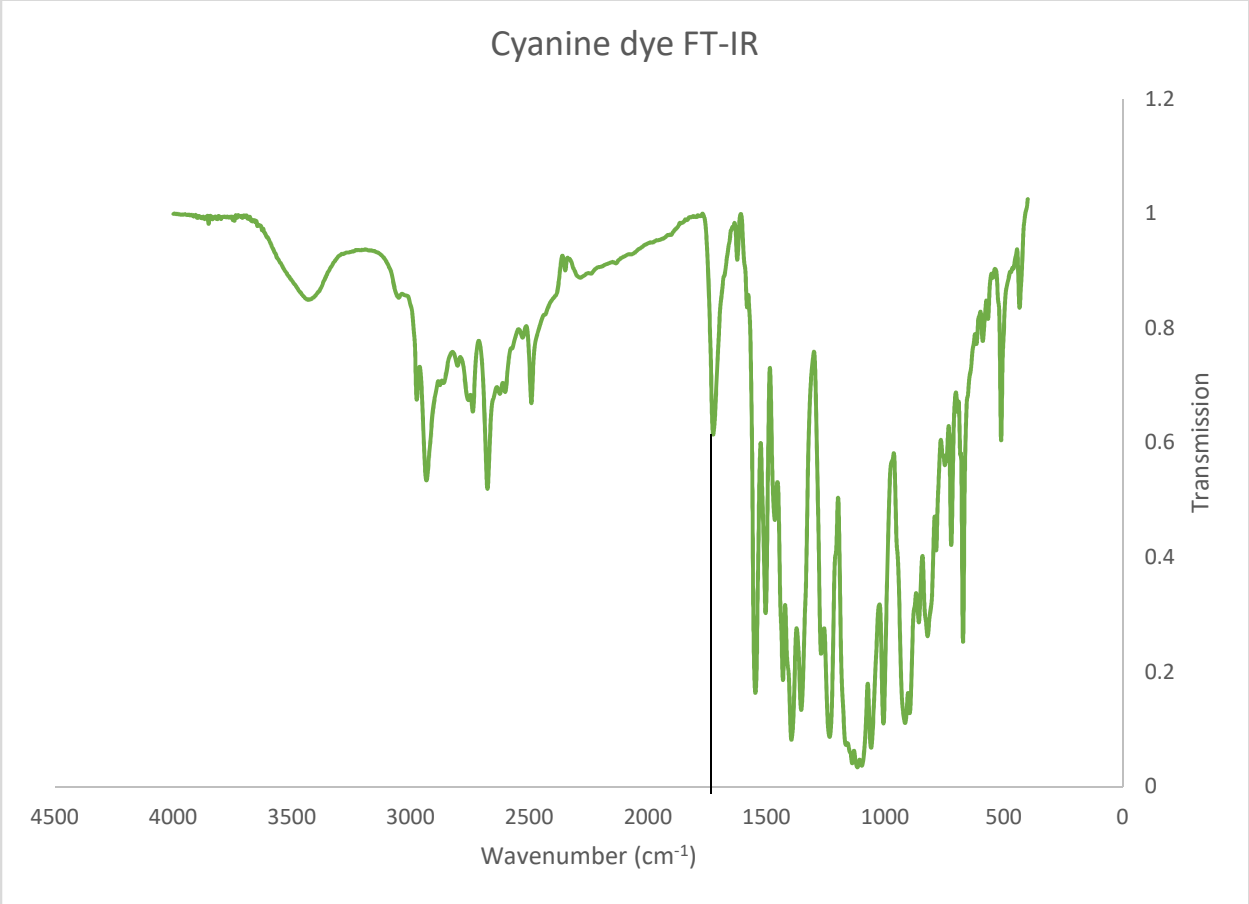

Figure 7.1 Cyanine dye infrared spectrum.

The dye exhibits many characteristic peaks, as expected for a complex organic chromophore. The feature of most interest lies at 1727 cm^{-1}, indicated in Figure 7.1. This peak is expected to be the one that is most perturbed when bound to the dye, as it relates to the symmetric C=O vibrational stretching frequency. When carbonyl groups bind to metal oxides, specifically ZnO, this stretching should be be confined and split into two COO^- stretching frequencies: one asymmetric stretch between 1500-1600 cm^{-1} and one symmetric stretch near 1400 cm^{-1}. This has been studied with respect to fatty acids containing carbonyl groups, before and after binding with metal oxides.[23]

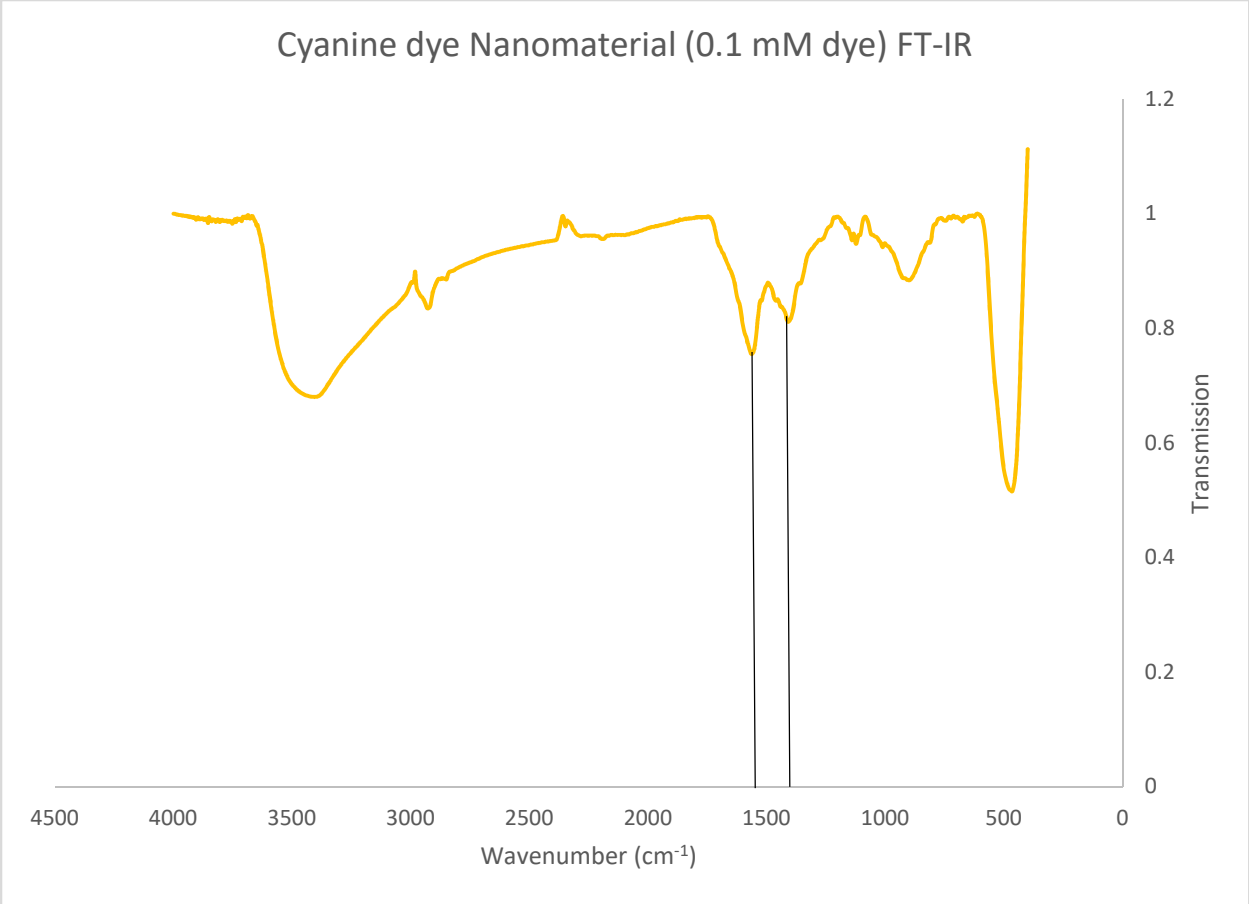

Figure 7.2 Nanomaterial (0.1 mM dye) infrared spectrum.

Unfortunately, the batch with 0.1 mM dye contained such a low concentration of dye that it is difficult to identify many of the characteristic dye peaks. In Figure 7.4, the FT-IR spectrum of ZnO is pictured, which strongly resembles the spectrum in Figure 7.2. Ideally, the nanomaterial spectrum should have the same cluster of peaks as the dye, but its intensity should be conflated by the ZnO spectrum. However, it can be observed that the carbonyl C=O stretch at 1727 cm^{-1} has disappeared, and does appear to be replaced by two stretches: one at 1560 cm^{-1} and one at 1400 cm^{-1}. This confirms the assumption that Zn binding will split the C=O stretch into asymmetric and symmetric COO^- stretches, but the peaks are small. More convincing data will be presented for sample 1.0 mM dye.

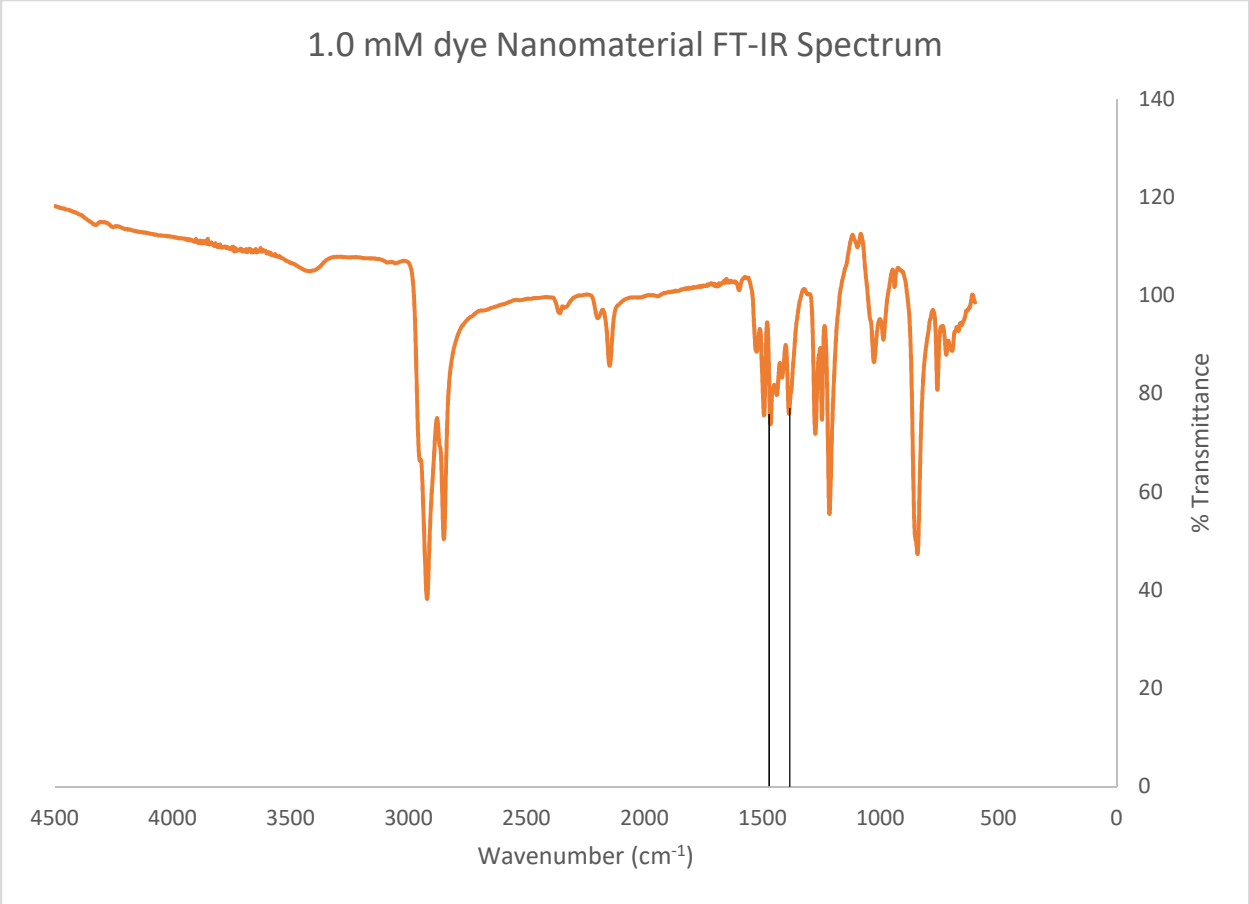

Figure 7.3 1.0 mM dye nanomaterial infrared spectrum.

Comparing the spectra shown in Figures 7.2 and 7.3 reveals clearly see the progressive effects of binding the dye to ZnO. The broad features of ZnO become sharper and more numerous, becoming conflated with the infrared spectra of cyanine dye and ZnO. The carbonyl C=O feature at 1727 cm^{-1} from the dye is the only feature which appears to be eliminated. It is instead split into two features, highlighted in Figure 7.3 at 1465 and 1387 cm^{-1}. The additional shift relative to Figure 7.2 is likely due to the further progression of binding in the more concentrated dye nanomaterial, increasing the level of confinement the carbonyls are subjected to and decreasing their vibrational frequencies.

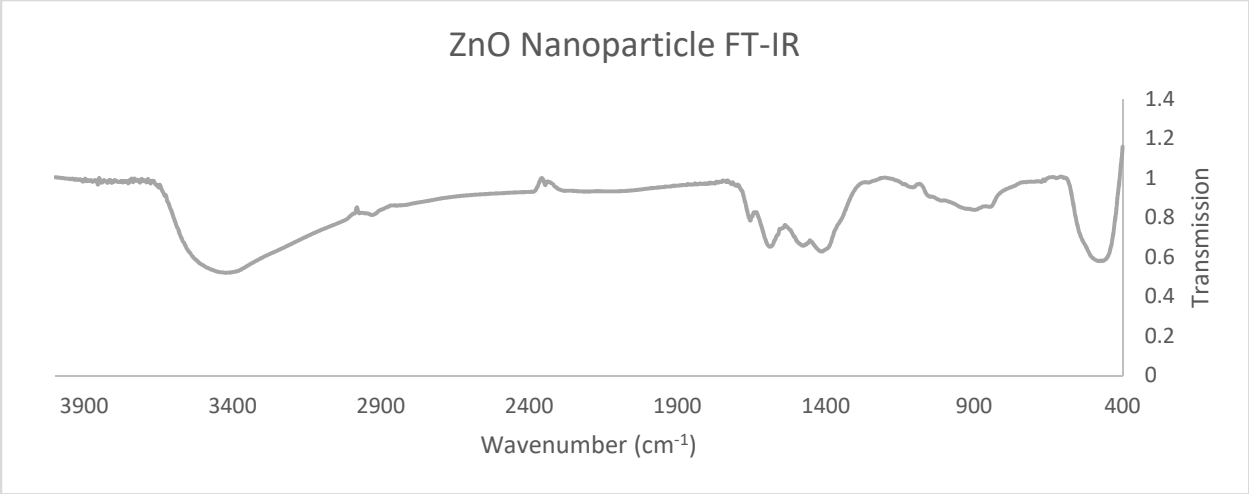

Figure 7.4 ZnO infrared spectrum.

As presented in Figure 7.4, the infrared spectrum of ZnO appears to be almost identical to that of batch 0.1 mM dye, indicating that the concentration of dye in the batch was in fact too weak to be properly detected by this technique. Normally, the infrared spectrum of ZnO should be relatively flat, as illustrated in Figure 7.5. However, the use of TBAB as surfactant introduces a range of covalent vibrational modes (1400-1650 cm^{-1}) near the fingerprint region

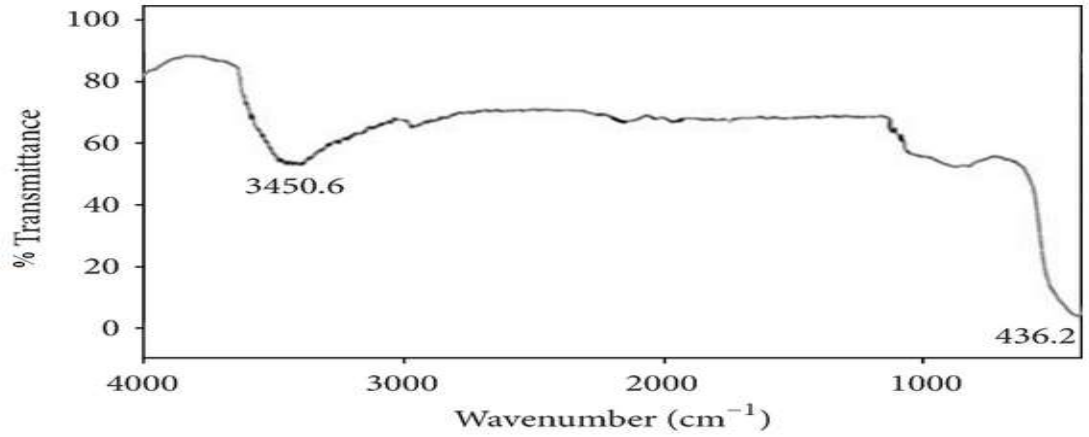

Figure 7.5 ZnO nanoparticle infrared spectrum.[22]

3.8. **Ultraviolet-Visible Spectroscopy (UV-Vis)**

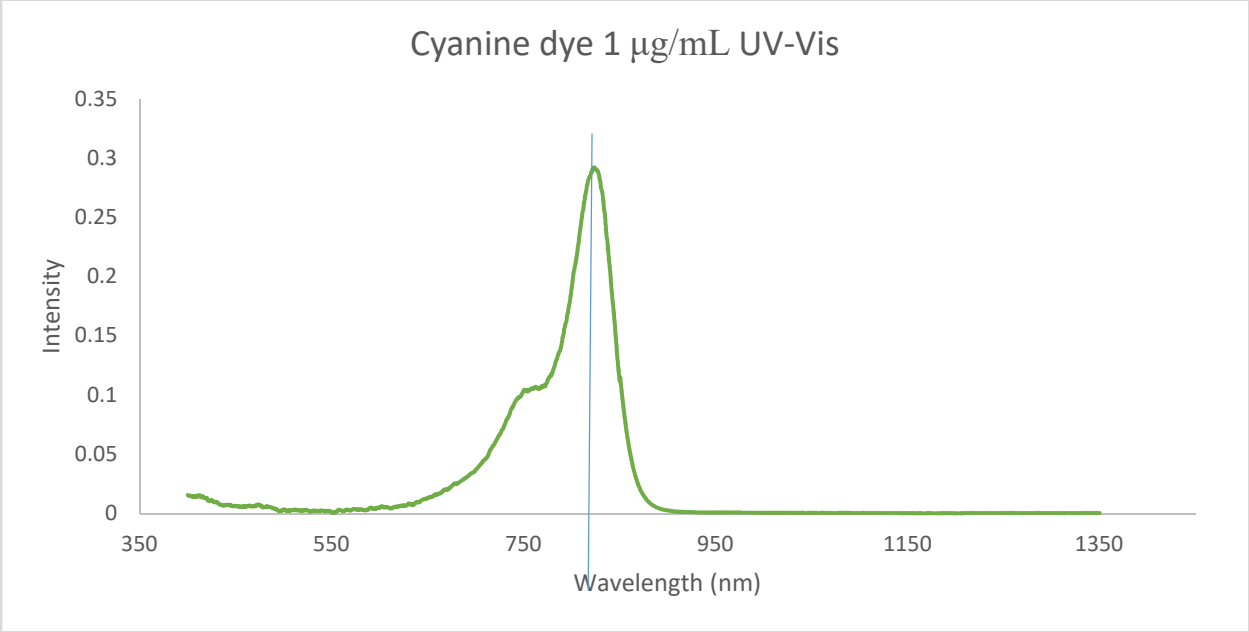

Figure 8.1 UV-Vis spectrum of cyanine dye.

As expected of a designer cyanine dye, a relatively narrow peak is observed near the predicted wavelength of 819 nm. The peak shown in Figure 8.1 appears at 823 nm. This peak should only be shifted by a few nm when bound to the ZnO nanoparticles.

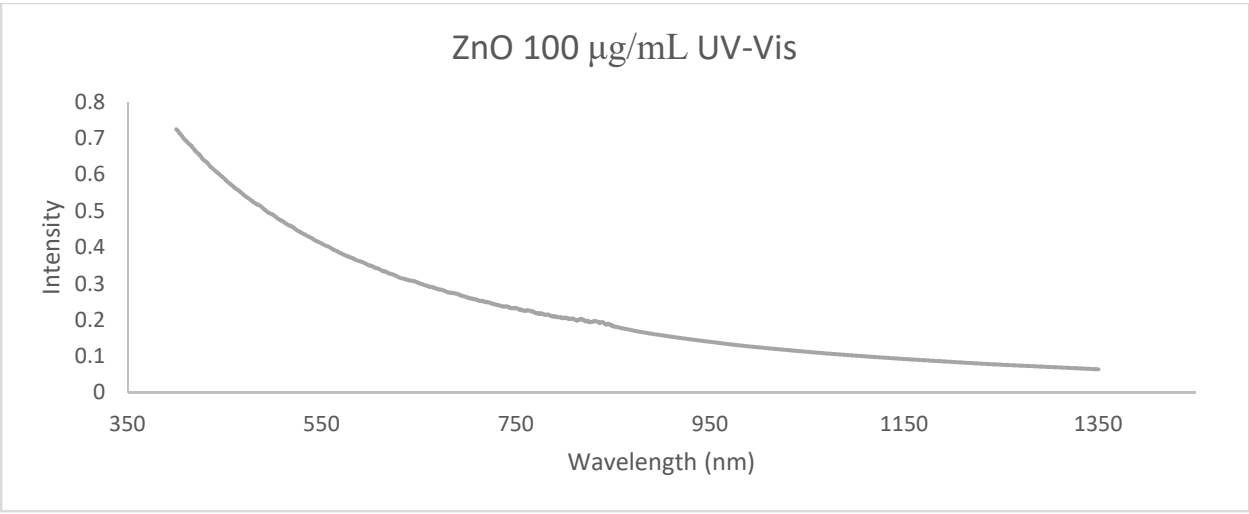

Figure 8.2 UV-Vis spectrum of ZnO nanoparticles.

The white ZnO nanoparticles show no characteristic peak, and instead show increased levels of absorbance at lower wavelengths due to scattering as the wavelength approaches the size of the nanoparticles.

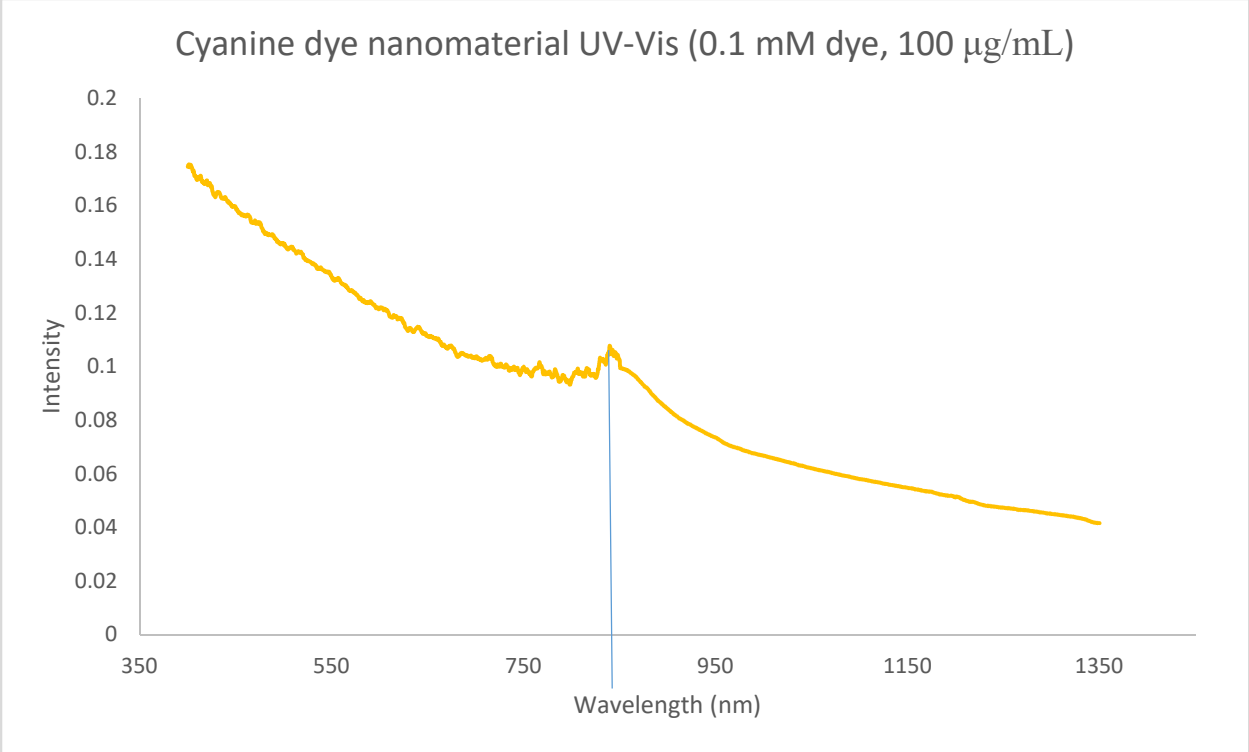

Figure 8.3 UV-Vis spectrum of nanomaterial (0.1 mM dye).

Due to the low concentration of dye, ZnO dominates this spectrum. Still visible is the dye peak, shifted to 840 nm, but it is extremely weak compared to the other features of the spectrum. This situation should be ameliorated with batch 1.0 mM dye with a full 1.0 mM dye solution, providing enough dye for a sufficient excess with respect to the nanoparticles and ensuring full coverage of the nanoparticle surfaces by the dye.

The next two spectra were recorded in plastic cuvettes using the Shimadzu UV-Vis spectrophotometer, which persistently revealed a broad absorbance strong at 900 nm

with a tail to 1350 nm. For comparison with cyanine dye, a new spectrum was recorded with dye in the Shimadzu UV-Vis to accurately compare the two spectra.

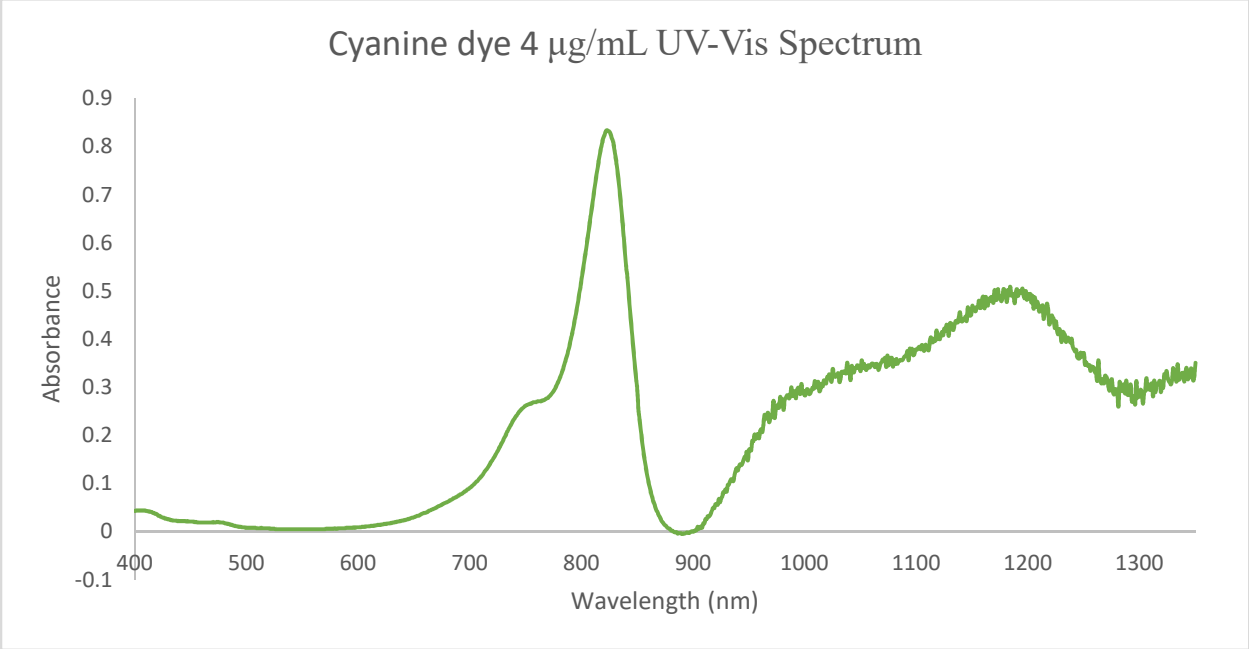

Figure 8.4 Shimadzu UV-Vis spectrum of cyanine dye.

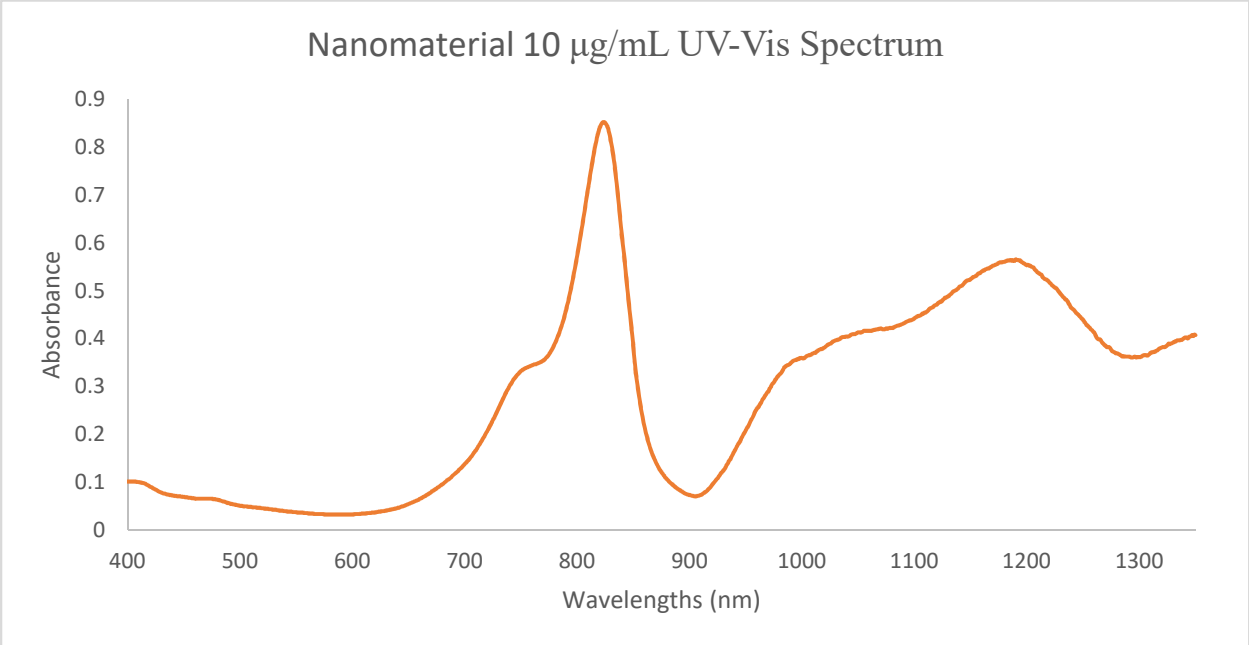

Figure 8.5 Shimadzu UV-Vis spectrum of 1.0 mM dye nanomaterial.

As seen in Figures 8.4 and 8.5, there is the same broad absorbance starting at 900 nm, but the characteristic feature at 825 nm occurs in both nanomaterial and dye, with a 5:2 ratio of concentration required for the same level of absorbance. The original UV-Vis spectrum of the dye is otherwise identical to the nanomaterial spectrum, indicating success in improving thermal stability without significantly altering the optical properties of the dye.

In order to ascertain the HOMO-LUMO gap of the nanomaterial and dye, the UV-Vis absorption data was made into a Tauc plot to examine the absorption threshold (Figures 8.6 and 8.7). The y-axis, whose title was obscured, was $(\alpha h\nu)^{-1/2}$ with units of $cm^{-1/2}$.

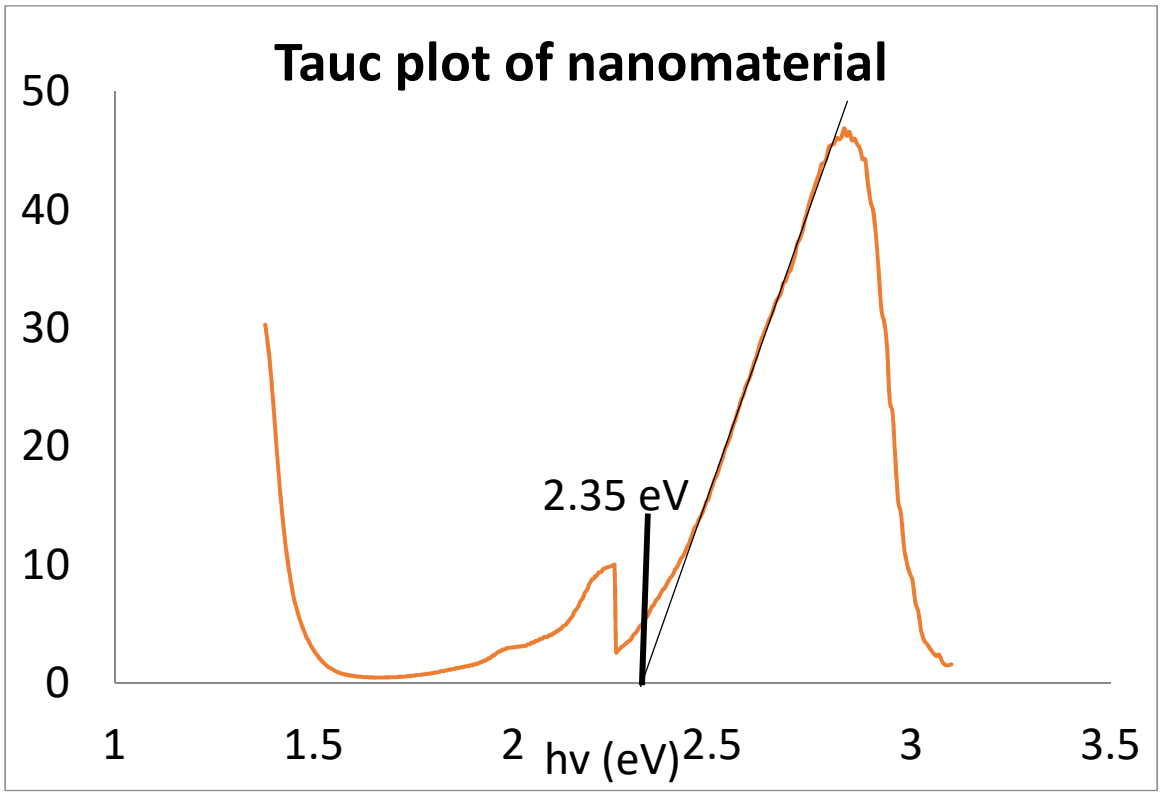

Figure 8.6 Tauc plot of nanomaterial.

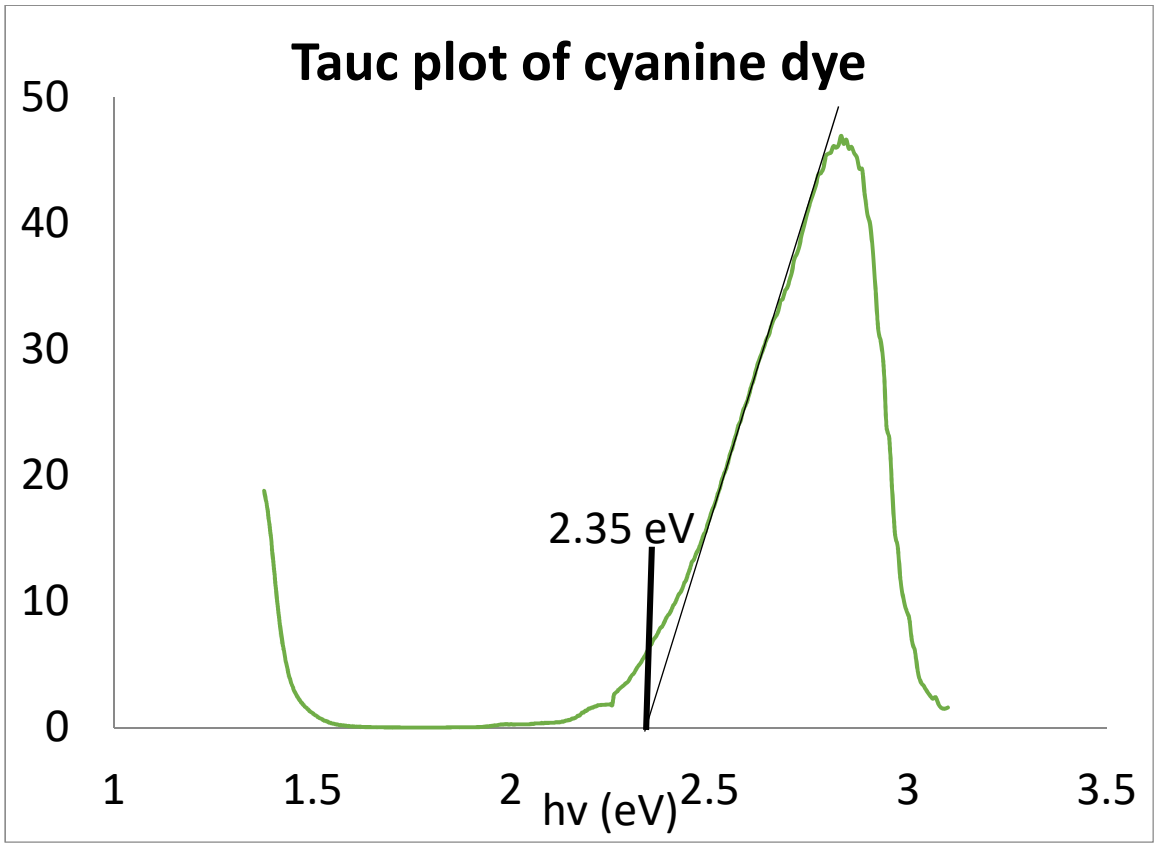

Figure 8.7 Tauc plot of cyanine dye.

As pictured in Figures 8.6 and 8.7, both the nanomaterial and the dye share the same HOMO-LUMO gap of approximately 2.35 eV. This confirms that the formation of the nanomaterial did not disrupt the characteristic optical properties of the cyanine dye.

4. Conclusions

In summary, there is conclusive evidence that ZnO has bound to the dye through the O_2C carboxylate functionality, as shown by the split peaks at 1465 and 1387 cm^{-1} in the FT-IR spectrum. Using Raman spectroscopy, it was also shown that the dye binds to the surface of ZnO nanoparticles, replacing the surfactant TBAB in the process. Through SEM and TEM imaging, it was possible to see the exact level of aggregation in the

nanoparticles, as well as the size of individual nanoparticles. In batch 1.0 mM dye, the particle size was fairly regular, ranging from 90-110 nm. These particles possessed a UV-Vis spectrum identical to the pure dye, with only a slight decrease in intensity of absorbance due to the increased molecular weight of the nanomaterial. Additionally, it retained the fluorescent peak of the dye, with an additional 5 nm blue shift shift due to the addition of ZnO. EDX analysis confirms the dominant presence of carbon in the nanomaterial due to the presence of dye, but also identified the chloride counter-ion from the dye and bromide counter-ion from the TBAB, both in trace quantities. Finally, through TGA and DSC analysis, it was revealed that the nanomaterial is significantly more thermally stable than the dye up to temperatures of 350 ºC, retaining almost six times more of its mass after heating than the naked dye. It is safe to conclude that this process of binding a dye in situ to ZnO nanoparticles is a cost-effective method of preserving its optical properties, while significantly increasing its thermal stability.

5. References

1. L. An, Z. Cai, W. Wang, J. Pu, Z. Li, *European Polymer Journal*, **2014**, *52*, 166-171.

2. K. Funabiki, K. Yagi, M. Nomoto, Y. Kubota, M. Matsui, *Journal of Fluorine Chemistry*, **2015**, *174*, 132-136.

3. M. A. Salvador, P. Almeida, L. V. Reis, P. F. Santos, *Dyes and Pigments*, **2009**, *82*, 118-123

4. K. Pydsinska, M. Ziółek, *Dyes and Pigments*, **2015**, *122*, 272-279.

5. M. Matsui, Y. Hashimoto, K. Funabiki, J-Y. Jin, T. Yoshida, H. Minoura, *Synthetic Materials*, **2005**, *148*, 147-153.

6. P. Sharma, S. Brown, G. Walter, S. Santra, B. Moudgil, *Advances in Colloid and Interface Science*, **2006**, *123-126*, 471-485.

7. T. Graen, M. Hoefling, H. Grubmüller, *Journal of Chemical Theory and Computation*, **2014**, *10*, 5505-5512.

8. J. Fablan, H. Nakazumi, M. Matsuoka, *Chemistry Reviews*, **1992**, *92*, 1197-1226.

9. K. Meral, M. Arık, Y. Onganer, *Journal of Molecular Structure,* **2016**, *1105*, 350-356.

10. J. L. Bricks, A. D. Kachkovskii, Y. L. Slominskii, A. O. Gerasov, S. V. Popov, *Dyes and Pigments*, **2015**, *121*, 238-255.

11. A. Tyagi, D. del Agua, A. Penskofer, O. García, R. Sastre, A. Costela, I. García -Moreno, *Chemical Physics*, **2007**, *342*, 201-214.

12. L. Yuan, W. Lin, K. Zheng, L. He, W. Huang, *Chemical Society Reviews*, **2013**, *42*, 622-661.

13. J. Rao, A. Dragulescu-Andrasi, H. Yao, *Current Opinion in Biotechnology*, **2007**, *18*, 17-25.

14. L. Josephson, M. F. Kircher, U. Mahmood, Y. Tang, R. Weissleder, *Bioconjugate Chemistry*, **2002**, *13*, 554-560.

15. C. Würth, D. Geißler, T. Behnke, M. Kaiser, U. Resch-Genger, *Analytical and Bioanalytical Chemistry,* **2015**, *407*, 59-78.

16. K. R. Karimullin, A. V. Naumov, *Journal of Luminescence,* **2014**, *152*, 15-22.

17. A. G. Karabadzhak, M. An, L. Yao, R. Langenbacher, A. Moshnikova, R-C. Adochite, O. A. Andreev, Y. K. Reshetnyak, D. M. Engelman, *ACS Chemical Biology*, **2014**, *9,* 2545-2553.

18. Skorenko, Kenneth H. PhD. Dissertation, State University of New York at Binghamton, 2015.

19. Z. L. Wang, *Journal of Physics: Condensed Matter*, **2004**, *16*, R829-R858.

20. Lee, Sunghee. Master's Thesis, State University of New York at Binghamton, 2011.

21. Skorenko, K.; Bernier, R.; Galusha, B.; Goroleski, F.; Bernier, W.; Jones, W.E. Increased Thermal Stability of Organic Chromophores with Nanoparticle ZnO. *Dyes and Pigments*, *Accepted Pending Publication*

22. M. Kooti, A. Naghdi Sedeh, *Journal of Chemistry*, **2012**, *2013*, 4 p.

23. V. Otero, D. Sanches, C. Montagner, M Vilarigues, L. Carlyle, J. A. Lopes, M. J. Melo, *Journal of Raman Spectroscopy*. **2014**, *45*, 1197–1206.

24. Brittanica. Dye. http://www.britannica.com/technology/dye (accessed April 27, 2016)

25. A-K. Kirchherr, A. Briel, K. Mäder, *Molecular Pharmaceutics*. **2009**, *6* (2), 480-491.

26. J. Liqiang, S. Xiaojun, S. Jing, C. Weimin, X. Zili, D. Yaoguo, F. Honggang, *Solar Energy Materials & Solar Cells*, **2003**, *79*, 133-151.

27. N. Saito, M. Akiba, Y. Inagaki, M. Shibata, T. Ishida, H. Kubo, *Japanese Journal of Applied Physics*, **2009**, *48*, 042402.

28. W. M. Nau, J. Mohanty, *International Journal of Photoenergy*, **2005**, *07*, 133-141.

29. A. Lenz, L. Selegård, F. Söderlind, A. Larsson, P. O. Holtz, K. Uvdal, L. Ojamäe, P-O. Käll, *Journal of Physical Chemistry C.* **2009**, *113* (40), 17332-17341.